

this Center. We also wish to thank Miss F. L. Cheng for help with the computations. We also

thank Dr. Crabtree, Dr. Ketterson, and Dr. Windmiller for sending us their data prior to publication.

- *Supported in part by the Advanced Research Projects Agency.
[†]Supported in part by the National Science Foundation.
¹L. F. Mattheiss, Phys. Rev. **139**, A1893 (1965).
²M. M. Halloran, J. M. Condon, J. E. Graebner, J. E. Kunzler, and F. S. L. Hsu, Phys. Rev. **B 1**, 369 (1970).
³G. B. Scott and M. Springford, Proc. R. Soc. A **320**, 115 (1970).
⁴N. E. Alekseevskii, K. Kh. Bertel, and A. V. Dubrovin, Zh. Eksp. Teor. Fiz. Pis'ma Red. **10**, 116 (1969) [JETP Lett. **10**, 74 (1969)].
⁵W. A. Reed and R. R. Soden, Phys. Rev. **173**, 677 (1968).
⁶E. Fawcett, W. A. Reed, and R. R. Soden, Phys. Rev. **159**, 533 (1967).
⁷R. A. Deegan and W. D. Twose, Phys. Rev. **164**, 997 (1967).
⁸L. F. Mattheiss, Phys. Rev. **B 1**, 373 (1970).
⁹J. C. Slater, Phys. Rev. **81**, 385 (1951).
¹⁰R. Gaspar, Acta Math. Acad. Sci. Hung. **3**, 263 (1954); W. Kohn and L. J. Sham, Phys. Rev. **140**, A1133 (1965).
¹¹J. R. Anderson and J. E. Schirber (unpublished).
¹²D. A. Papaconstantopoulos, J. R. Anderson, and J. W. McCaffrey, Phys. Rev. **B 5**, 1214 (1971).
¹³J. O. Dimmock, Solid State Phys. **26**, 103 (1971).
¹⁴T. L. Loucks, *Augmented-Plane-Wave Method* (Benjamin, New York, 1967).
¹⁵L. F. Mattheiss, J. H. Wood, and A. C. Switendick, Methods Comput. Phys. **8**, 63 (1968).
¹⁶W. B. Pearson, *Lattice Spacings and Structure of Metals and Alloys* (Pergamon, New York, 1958).
¹⁷J. E. Holliday, in *The Electron Microprobe*, edited by T. D. McKinley, K. F. J. Meinrich, and D. B. Wittry (Wiley, New York, 1966), p. 10.
¹⁸V. V. Nemoshkalenko and V. P. Krivitskii, Ukr. Fiz. Zh. **13**, 1274 (1968) [Ukr. Phys. J. **13**, 911 (1969)].
¹⁹D. E. Eastman, Solid State Commun. **7**, 1697 (1969).
²⁰F. Heininger, E. Bucher, and J. Muller, Phys. Kondens. Mater. **5**, 243 (1966).
²¹W. L. McMillan, Phys. Rev. **167**, 331 (1968).
²²T. F. Smith, Phys. Lett. A **33**, 465 (1970).
²³G. Crabtree, J. B. Ketterson, and L. R. Windmiller (private communication).
²⁴The compressibility K_T of Nb at 4.2 °K has been obtained from the elastic constants of K. J. Carroll [J. Appl. Phys. **36**, 3689 (1965)]. The value is 5.78×10^{-4} kbar⁻¹.
²⁵J. F. Janak, A. R. Williams, and V. L. Moruzzi, Phys. Rev. **B 6**, 4367 (1972).

Probing the Electron-Phonon Interaction in Potassium by Far-Infrared Cyclotron Resonance

S. J. Allen, Jr., L. W. Rupp, Jr., and P. H. Schmidt

Bell Laboratories, Murray Hill, New Jersey 07974

(Received 29 November 1972)

To probe the electron-phonon interaction in potassium, Azbel'-Kaner cyclotron resonance has been observed at four frequencies in the far infrared (29.69, 32.12, 45.407, and 58.25 cm⁻¹). The experiments were performed on a novel reflection cavity spectrometer with balanced homodyne detection driven by a c.w. far-infrared laser. Signals are seen for E₁H and E₂H at 29.69 and 32.12 cm⁻¹, but only for E₁H at 45.407 and 58.25 cm⁻¹. Two effects distinguish cyclotron resonance in potassium in the infrared from that observed at microwaves. First, since the resonant electron does not escape the skin depth before the infrared field changes phase, the resonances suffer from retardation effects and are no longer amenable to the usual Azbel'-Kaner or Chambers theory of cyclotron resonance. Second, there is a strong enhancement of the electron-phonon relaxation rate due to the large density of phonon states available to scatter the excitations when the laser frequency is near the Debye frequency, ≈ 75 cm⁻¹. The line-shape analysis, used to extract the electron-phonon coupling parameter λ , does not reproduce all of the observed features. In particular, it does not reproduce absorption features on the high-field side of the subharmonic resonance which are shown to be related to the cyclotron waves that propagate across the magnetic field in the bulk. Nevertheless, by focusing attention on the breadth and position of the leading edge of the resonance, we can extract an electron-phonon λ . λ is found to be 0.11 ± 0.02 and agrees with that determined by the temperature dependence of the phonon-limited dc resistivity.

I. INTRODUCTION

Electrons in normal metals form a strongly interacting gas whose transport properties are best formulated in terms of quasiparticles.¹ Quasiparticles, as conceived by Landau,^{1,2} represent

the low-lying collective excitations of the interacting electron system, and behave very much like the electrons from which they were constructed—with one important exception. Whereas the electron lifetime is extremely short, the quasiparticle motion is long lived. Since the quasiparticle state is

well defined, the concept enables us to understand qualitatively why transport in normal metals can be well described by a nearly-free-electron gas. The two basic many-body interactions in metals, the Coulomb interaction between electrons, and the interaction between the electron and phonon, are not removed by the transformation from electrons to quasiparticles but are reexpressed in terms of the quasiparticle excitations.

These interactions are formulated in two different ways depending on whether the excitations are on the Fermi surface or make large excursions from it. First, the energy of a collection of quasiparticles is said to depend on the distribution of quasiparticles as well as the sum of the energies of the individual particles. This is phenomenologically described in terms of the Landau scattering function^{1,2} and is relevant to excitations with energies that are much less than either the Coulomb interaction energy or phonon Debye energy. The structure of the scattering function has been probed experimentally with cyclotron waves by Walsh and Platzman³⁻⁵ and with spin waves by Schultz and Dunifer.⁶ Secondly, for excitations that have a finite energy above the Fermi energy E_F , one expects that the simple relation between energy and momentum $E(p) = p^2/2m$ will no longer hold. In particular, theory states that one adds an energy-dependent correction $\Sigma(E - E_F)$, which is called the self-energy.⁷ The self-energy modifies the energy momentum relationship at the Fermi level, producing a shift in mass and at finite energies a finite quasiparticle lifetime. Σ has structure at an energy characteristic of the interaction that produced it. In particular, the electron-phonon part produces structure at the Debye energy, approximately 10^{-2} eV, whereas the Coulomb part contributes structure only at energies near 1 eV. In the present discussion we are only concerned with energies up to the Debye energy so that we can expose the electron-phonon part in the following way^{8,9}:

$$E(p) = p^2/2m_c + \Sigma_{e-p}(E - E_F). \quad (1)$$

In (1) we have replaced the bare mass with the mass dressed by the Coulomb interaction, and the electron-phonon contribution to the self-energy, $\Sigma_{e-p}(E)$, is calculated in the presence of all the electron-electron interactions. The object of the present experiments is to make experimental contact with the real and imaginary parts of $\Sigma_{e-p}(E)$ by observing Azbel'-Kaner¹⁰ cyclotron resonance near the Debye frequency in potassium, an experiment first proposed by Scher and Holstein.^{11,12}

There are, of course, a number of other experimental probes of the electron-phonon coupling in metals. The most effective probe of the electron-phonon self-energy has been and is the tunneling measurement with a strong-coupling superconduc-

tor.¹³ Although it is restricted to strong-coupling superconductors, and the self-energy measured this way is suitably averaged over the Fermi surface, the information obtained using this technique far exceeds that obtained with any other spectroscopic probe of the electron-phonon system. Temperature-dependent cyclotron¹⁴ and surface-state¹⁵ resonances measure the temperature dependence of the self-energy, usually the imaginary part, from an experimentally determined scattering rate,¹⁵⁻²¹ but recently the real part, from temperature-dependent mass shifts as reported by Sabo,¹⁸ Goy,¹⁹ Poulsen and Datars,²⁰ and Krasnopolin and Kaikin.²¹ Where such comparisons can be made, the electron-phonon interaction, deduced from these temperature-dependent effects, agrees with measurements obtained from tunneling experiments.

Electromagnetic spectroscopy of the self-energy has been hindered by the fact that the frequency range of interest, near the Debye frequency, is not conducive to the sensitive spectroscopy required to observe weak absorptive changes in metals. Despite these difficulties, Joyce and Richards²² have observed the Holstein²³ volume absorption in superconducting lead, which is the phonon-aided electromagnetic absorption by electrons. Further, Goy and co-workers^{19,24} have observed frequency-dependent masses and lifetimes in Hg, Pb, and In by observing Azbel'-Kaner¹⁰ cyclotron resonance at frequencies as high as 15 cm^{-1} . In the latter measurements, the correct frequency dependences are obtained, but the magnitude of the shifts are less than expected from the tunneling data on these same materials. The source of this discrepancy is not understood at this time.

The experiments described herein observe cyclotron resonance in potassium at 29.69, 32.12, 45.407, and 58.25 cm^{-1} . Although 15 cm^{-1} short of the Debye peak in the phonon density of states, all four frequencies excite electron-hole pairs that sample an appreciable phonon density of states and effects due to the frequency dependence of the self-energy should manifest themselves in the lifetime, if not the effective mass. Unlike the systems studied to date by high-frequency cyclotron resonance, potassium is a weakly coupled electron-phonon system not suited to tunneling spectroscopy. Experimental measure of the electron-phonon coupling can be made, however, by a detailed analysis of the temperature-dependent resistivity.²⁵⁻³² We return to this work in Sec. V. The case for studying self-energy or electron-phonon effects by high-frequency cyclotron resonance in potassium is most strongly supported by its being the archetypal normal metal whose simplicity makes a confrontation between theory and experiment hard to avoid. It has been extensively studied both theoretically^{33,34}

and experimentally.^{3-6,35,36} An extremely precise value of the microwave mass $m^*/m = 1.217 \pm 0.002$, has recently been determined by Walsh³⁷ and is invaluable for this work.

Quite apart from understanding the self-energy corrections, the simple spherical Fermi surface³⁶ is important from another point of view. Cyclotron resonance in the far infrared does not appear to be properly described by either the Azbel'-Kaner¹⁰ or Chambers theory³⁸ and suffers so-called retardation effects.³⁹⁻⁴¹ Consequently, as one extends the frequency into the far infrared, not one, but two effects set in. Not only are there changes in the self-energy, which manifest themselves as a mass shift and increase in linewidth, and are of primary interest here, but there are also changes in the electrostatics of the semi-infinite metal in a magnetic field. Separating these two effects is crucial to extracting any meaningful self-energy parameters. [In this regard we note that in far-infrared cyclotron-resonance experiments in Cu⁴² and Be,⁴³ one obtains anomalous shifts in the cyclotron mass that are not related to the frequency dependence of the self-energy. In the case of copper it appears that, whereas a $\langle 100 \rangle$ directed field gives strong belly-orbit ($k_H = 0$) signals at microwave frequencies, the same orientation gives strong signals from another part of the Fermi surface in the far infrared. Clearly these effects, though poorly understood, are related to Fermi-surface topology and can only confuse attempts to extract unambiguous changes in the electron-phonon self-energy. Potassium should be free of such ambiguities.]

In Sec. II we describe the experimental apparatus that was developed to make these experiments, while Sec. III describes the results. Section IV attempts to analyze the experimental results for the electron-phonon matrix element. This requires understanding the electrostatics of a semi-infinite metal in a magnetic field in the retardation regime. Since our understanding is rather poor, complete line-shape analysis is impossible. However, the electron-phonon coupling can be deduced if certain assumptions are made. In Sec. V the results of the experiment and analysis are summarized and discussed in the light of other experimental measurements and theoretical estimates of the electron-phonon coupling in potassium.

II. EXPERIMENTAL TECHNIQUE

The basic experimental problem involved in doing electromagnetic spectroscopy in metals is due to the dielectric impedance mismatch between the metal and free space. Assume we have radiation incident on a metal surface. The power reflectivity is

$$R = \left| \frac{Z - Z_0}{Z + Z_0} \right|^2, \quad (2)$$

where Z is the surface impedance of the metal and Z_0 the impedance of free space. If $Z \ll Z_0$, which is the case for all real metals, then

$$R \approx 1 - 4 \frac{\text{Re}(Z)}{Z_0} \quad (3)$$

and the change in reflectivity produced by a small change in real surface impedance is

$$\delta R = 4 \frac{\text{Re}(Z)}{Z_0} \frac{\delta \text{Re}(Z)}{\text{Re}(Z)}. \quad (4)$$

Since the impedance mismatch at the surface $\text{Re}(Z)/Z_0$ is usually of the order of 10^{-2} - 10^{-3} , in order to see 1% changes in surface impedance, changes in R of the order of 10^{-5} must be detected. The problem is further compounded in the far infrared, between 10 and 100 cm^{-1} , because spectroscopic techniques that are used successfully at lower frequencies (microwaves) and higher frequencies (optical and infrared), fail. (In fact, most successful spectroscopic systems, in this transition region of the spectrum, are a strange marriage of optical and microwave techniques.)

Despite the difficulty involved in doing spectroscopy in metals in the far infrared, there are documented a number of successful approaches to this problem worth noting here. Although not a bulk measurement, the first experiments on metals in the far infrared are reported by Glover and Tinkham,^{44,45} who measured transmission on thin superconducting and normal lead films. Absorption in bulk superconductors in the far infrared was first observed by Richards and Tinkham⁴⁶ by measuring the energy density in a nonresonant cavity made of the superconductor under study. In these experiments many bounces from the surface helped overcome the impedance mismatch between the metal and free space. Direct absorption experiments, performed by measuring the temperature change in the sample produced by far-infrared radiation falling directly on the sample, have been used successfully to measure both the energy gap in superconductors⁴⁷ as well as the structure above the gap related to the Holstein volume absorption.²² Particularly relevant to the present paper is the use of the direct absorption technique by Goy and Weisbuch⁴⁸ and Goy *et al.*¹⁹ to observe cyclotron resonance in real metals at frequencies as high as 15 cm^{-1} . Lastly, we note the rather ingenious transmission line geometry developed by Drew and Sievers⁴⁹ and recently exploited by Strom, Drew, and Koch⁵⁰ to do cyclotron resonance in semimetals in the far infrared.

Although the experimental apparatus used in the current experiments is quite different from tech-

niques used heretofore in the far infrared, it is similar to microwave spectrometers used to do reflection spectroscopy in metals and is, in fact, a far-infrared analog of a reflection cavity spectrometer with balanced homodyne or bridge detection. A schematic diagram of the optical part of the system is shown in Fig. 1.

The source of radiation is a cw far-infrared laser filled with any one of a number of gases or vapors to provide five frequencies in far infrared, 29.69, 32.12, ⁵¹⁻⁵⁴ 45.407, 58.25, and 84.32 cm^{-1} .⁵⁵ (Higher frequencies can be obtained with the laser but have not been used with the spectrometer.) The laser resonator consists of a spherical mirror with ~ 4 -m focal length and a flat mirror with a 1-mm hole for coupling out radiation. The separation between mirrors is ~ 4 m and the inside diameter of the Pyrex water-cooled tube is ~ 10 cm. Typical power levels obtained from the laser are $\sim 1 \mu\text{W}$. Although considerably more power can be obtained at the HCN frequencies of 29.69 and 32.12 cm^{-1} , no attempt is made to do so for two reasons. First, microwatts are adequate to do the spectroscopy and second the clean-up operation following operation with the cyanide (a necessity in order to obtain oscillation on the H_2O or D_2O) is easier if the laser is run at minimum cyanide and electrical power levels.

There are two essential elements in the spectrometer that will be described in detail—the cavity and the balanced bridge. The cavity, of course, attempts to overcome the dielectric mismatch between the metal sample and free space. The Q of the cavity used in these experiments is sufficiently high that changes in reflectivity of the cavity, due to changes in surface impedance of the sample, are 100 times as large as would be seen from the bare metal. The cavity is placed in one arm of a double Michelson interferometer which is tuned in such a way that changes in cavity reflectivity will unbalance the signals at the two detectors. With

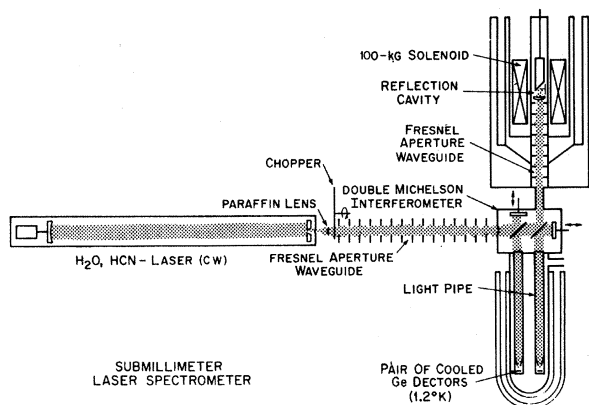


FIG. 1. Optical part of the far-infrared laser spectrometer.

some care, short-term changes as small as 10^4 can be seen with a 1-sec integration time. The bridge-cavity system appears to be able to detect changes as small as $1/10^6$ in reflectivity in the sample. Field modulation is not employed, although in principle there is nothing to prevent one from doing so.

A detailed sketch of the nearly concentric Fabry-Perot reflection cavity is shown in Fig. 2. Figure 2(a) shows the actual geometry while 2(b) shows an unfolded version with theoretical mode profile. The resonator is bounded by a curved 1000-line/in. copper screen⁵⁶ and the sample surface. The design of the cavity follows the analysis of Boyd and Gordon for the confocal resonator.⁵⁷ Minimum diffraction losses in a Fabry-Perot resonator are achieved in the confocal geometry, i. e., when the midplane of a two-curved-mirror system is the focal plane for both mirrors or in a spherical-planar system when the plane mirror is at the focal position of the spherical mirror. The plane mirror need not be placed at the focal plane, however, but may, in fact, be located at any point inside the radius of curvature. As one moves the plane mirror from the focal plane to the center of curvature, the diffraction losses increase until at the radius of curvature the resonator ceases to resonate.

Despite the increased diffraction losses, there are some good reasons for operating with a non-confocal geometry. We operate this resonator just inside the radius of curvature for two reasons. First, the spot size on the sample becomes arbitrarily small as one moves the sample or plane reflector near the concentric position. This allows the use of small samples. Indeed, samples as small as 2 mm on a side have been used in this geometry. Second, as the spot size on the sample becomes small, the spot size on the curved screen becomes large. This enables us to more nearly match the beam size on the screen with the profile of the incident radiation. To provide optimum coupling into the resonant cavity mode, they should be the same size.

Some numbers make the point more clear. In Fig. 3 we plot beam radius at the screen and sample as the screen sample separation approaches the radius of curvature. One notes that the beam radius at the sample goes to zero and the radius at the screen becomes large at the critical separation. We also note by arrows the beam radii for a true confocal system which would correspond to 0.5 on the abscissa. They are poorly suited to the sample and incident beam radii that we use in the experiment. The beam radius in the Fresnel guide is ~ 0.4 cm at 45 cm^{-1} , considerably less than the guide radius, and matches quite well the ~ 0.3 -cm beam radius in the cavity. The 25% difference in size should give an overlap of guide beam profile

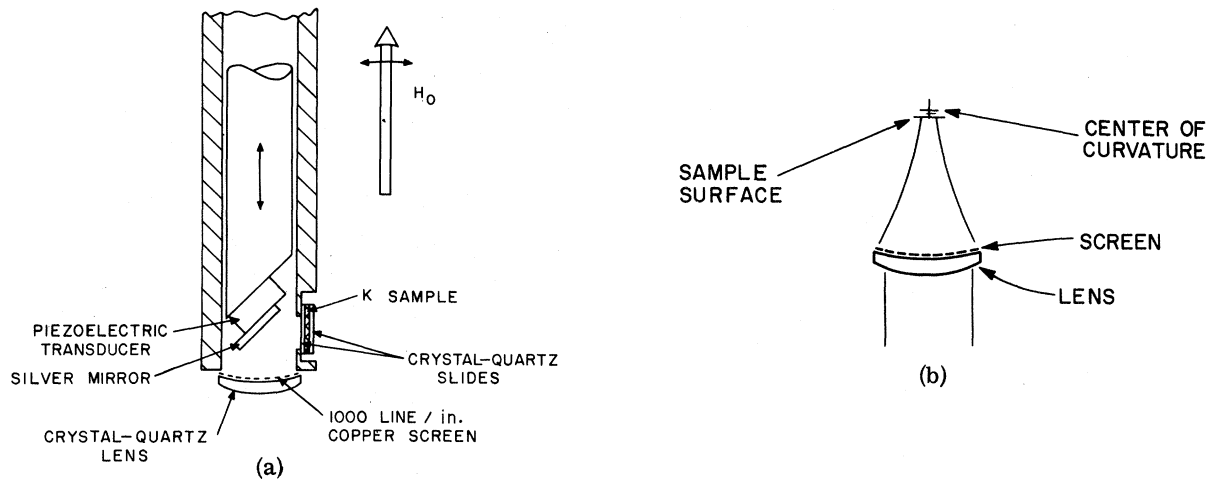


FIG. 2. (a) Nearly concentric Fabry-Perot reflection cavity. (b) Unfolded version of same showing the mode profile.

and cavity beam profile of 0.92, that is to say, 92% of the incident radiation will be coupled into the resonant mode. At the top of the figure the log of the loss per pass due to diffraction is plotted versus the screen sample separation. At $\alpha_D = 10^{-2}$ the diffraction loss is estimated to be equal to the other losses in the system, so that diffraction losses are expected to be appreciable only within one or two mode spacings of the critical separation. Experimentally one finds that diffraction losses are appreciable about four mode spacings from the critical separation.

The crystal-quartz lens serves to match the nearly-plane-wave front propagating up the Fresnel guide to the spherical-mode pattern emanating from the cavity. It is estimated that the lens must match the radius of curvature of the incoming wave to that of the screen to within $\pm 4\%$, to assure at least 80% of the incident radiation is coupled into the resonant mode.

Many of the above design criteria have not been confirmed experimentally, but the cavity system, shown in Fig. 2, was constructed along these lines and operates successfully. If we can consider the grid as being purely inductive,⁵⁸⁻⁶⁰ which it undoubtedly is not, then the magnitude of the reflection coefficient is just

$$\Gamma = \left(\frac{(r_s - r_m)^2 + 4r_s r_m \sin^2 \varphi / 2}{(1 - r_s r_m)^2 + 4r_s r_m \sin^2 \varphi / 2} \right)^{1/2}, \quad (5)$$

where r_s and r_m are the reflection coefficients of the screen and metal sample, respectively, and φ is the tuning parameter equal to $4\pi x / \lambda$, where x is the separation and λ the wavelength. On resonance at 45.407 cm^{-1} one obtains a $\Gamma \sim 0.1-0.6$, indicating that $r_s \approx r_m$. From the full width of the tuning peak, $\approx 0.2 \mu\text{m}$ at 45.407 cm^{-1} , one can deduce that $r_s \approx r_m \approx 0.995$, so that on resonance

$$\frac{\partial \Gamma}{\partial r_m} = - \frac{(1 - r_s^2)}{(1 - r_s r_m)^2} \approx -100. \quad (6)$$

A decrease in sample reflectivity is reflected in a 100-fold increase in cavity reflection coefficient. Although the quantitative description above refers to operation at 45.407 cm^{-1} , where optimum operation is obtained, the cavity is sufficiently broadband to be effectively used from 29 to 84 cm^{-1} .

During operation the cavity is electrically fine tuned with a piezoelectric stack producing a deflection of $\sim 0.3 \mu\text{m}$ for 200 V applied. An 80-Hz signal is simultaneously applied, and used in a suitable detection and feed-back circuit, to lock the cavity to the laser.

A schematic diagram of the bridge is shown in Fig. 4. It consists of two Michelson interferometers in tandem. The beam splitters are made of 0.001-in. Mylar. The right-most arm of the bridge is adjusted to transmit maximum power to the detector below it, and under these conditions it is easily shown that changes in power at this detector measure changes in the magnitude of the cavity reflection coefficient. The second interferometer provides a reference signal which is used to cancel the total signal to zero. This interferometer is tuned to give maximum power on the reference detector, for in this mode a change in reflectivity of the cavity will produce an opposite signal from that produced in the signal detector. It is, however, smaller than that produced in the signal detector. The amplitude and phase of the reference signal are adjusted to cancel the signal detector by adjusting reference-detector bias current and trimming it with a variable capacitor.

The two detectors are cooled ($\sim 1.2 \text{ }^\circ\text{K}$) Ga-doped-Ge bolometers⁶¹ with time constants $\leq 1 \text{ msec}$. They are capable of detecting of the order

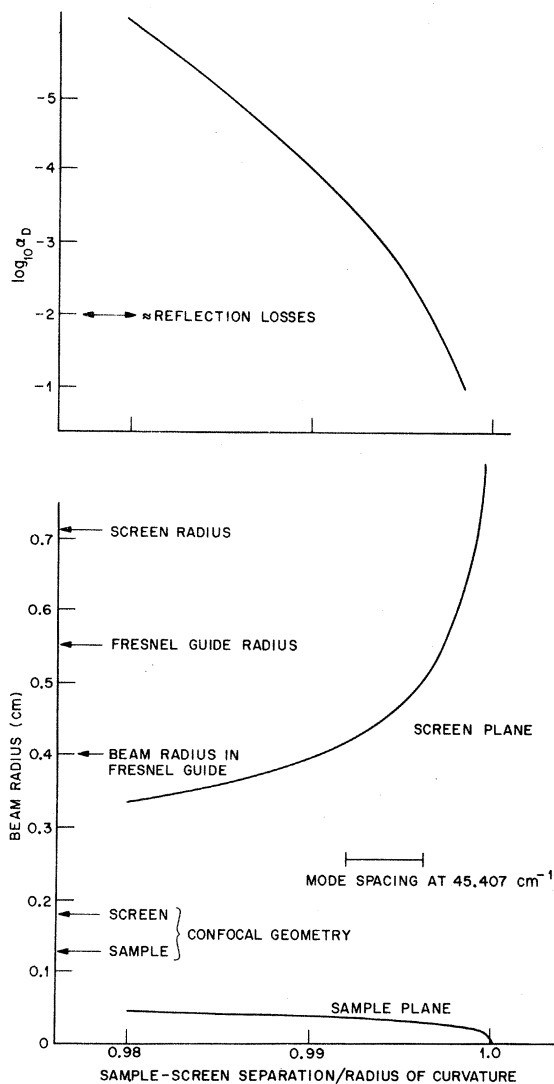


FIG. 3. Beam radius in the cavity as a function of screen-sample separation following Boyd and Gordon (Ref. 57). Also shown is the diffraction loss per pass, α_D , and a number of other relevant parameters.

of 10^{-10} – 10^{-11} W, but under normal operating conditions, with at least $1 \mu\text{W}$ of laser power, most of the noise in the system comes from low-frequency microphonics which either unbalance the bridge or detune the cavity.

Fresnel waveguides⁶² are used to minimize diffraction losses. They are no more than zeroth-order Fresnel lenses. Although not as efficient as light pipes,⁶³ they preserve spacial coherence, which is essential to the operation of the system. Lens waveguides with lower diffraction losses can be constructed but the reflection and absorption losses become prohibitive.⁶⁴ Multilayer interference filters constructed from high-purity Si and air are used to remove unwanted laser lines.

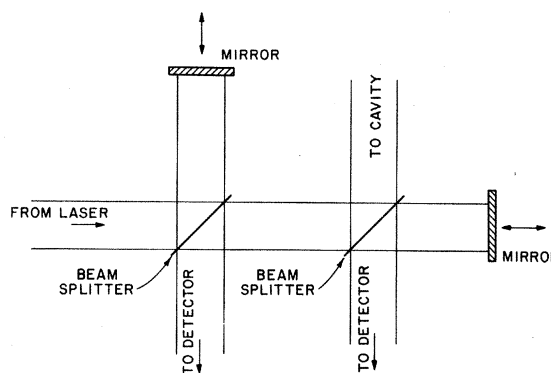


FIG. 4. Double Michelson interferometer.

Proper polarization is obtained by means of a rotatable 1000-line/in. grid on a Mylar substrate.

The sample used in these experiments was made from distilled potassium of resistivity ratio $\rho_{295}/\rho_{4.2} \approx 10000$, pressed between crystal-quartz plates, 0.0105-in. thick, forming a sample $12 \times 6 \times 0.1$ mm. Approximately 0.1 Torr of exchange gas cooled the sample to within 0.5°K of 4.2°K . The magnetic field could be tipped $\pm 0.8^\circ$ about the axis of the Dewar. The tipping excursion was sufficiently small to require care in loading the sample but large enough to observe tipping effects for those signals where alignment is crucial.

III. EXPERIMENTAL RESULTS

The data obtained for E (far infrared) parallel and perpendicular to the dc magnetic field is shown in Figs. 5–10. The data at 45.407 and 58.25 cm^{-1} are nine-run averages. The best performance of the system is obtained at 45.407 cm^{-1} , and in Fig. 11 we show a single run at 45.407 cm^{-1} with a 0.3-sec time constant. The corresponding changes in sample reflectivity and surface impedance are shown in the left of the figure. The noise corresponds to a $\sim 1/10^6$ change in reflectivity or $\sim 1/10^3$ change in surface impedance.

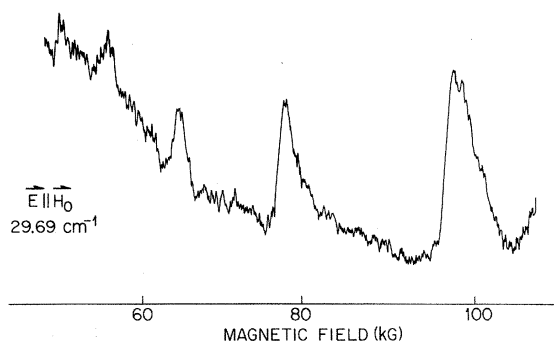


FIG. 5. Real surface impedance versus magnetic field, 4.2°K , 29.69 cm^{-1} , $\vec{E} \parallel \vec{H}$.

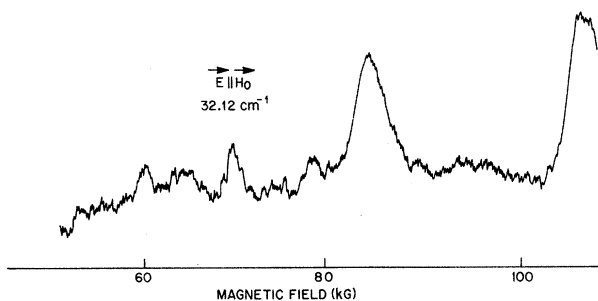


FIG. 6. Real surface impedance versus magnetic field, 4.2°K, 32.12 cm^{-1} , $\vec{E} \parallel \vec{H}$.

The orientation of the magnetic field with respect to the sample surface can play havoc with Azbel'-Kaner cyclotron resonance. In the far infrared, in potassium, we find that $\pm 0.8^\circ$ tip has no effect on cyclotron resonance for $\vec{E} \perp \vec{H}$ but does effect the $\vec{E} \parallel \vec{H}$ signals. In Fig. 12 we show the fourth subharmonic at 29.69 cm^{-1} as a function of field tip. The strong tip dependence for $\vec{E} \parallel \vec{H}$ and weak dependence for $\vec{E} \perp \vec{H}$ are understood qualitatively. Radiation with $\vec{E} \parallel \vec{H}$ delivers energy only to those electrons with finite velocity parallel to the magnetic field. In tipped magnetic fields, these electrons rapidly leave the skin depth and hence the line is broadened and shifted or split.^{65,66} On the other hand, the $\vec{E} \perp \vec{H}$ signals are dominated by electrons with no drift velocity along the field and consequently are less affected by tipping the magnetic field. From the symmetry of the tipping pattern (Fig. 12), we experimentally determine the field parallel position and estimate that we are aligned to within $\pm 0.1^\circ$.

The data are generally characterized by the usual subharmonic structure with a strong attenuation of the subharmonics due to retardation effects.³⁹ The $\vec{E} \parallel \vec{H}$ signals are weaker by approximately one order of magnitude, which is consistent with cyclotron resonance in the retardation regime. As we noted above, the $\vec{E} \parallel \vec{H}$ signals involve electrons with finite drift velocity parallel to \vec{H} and consequently smaller real-space orbits. Small real-space orbits attenuate the cyclotron resonance in

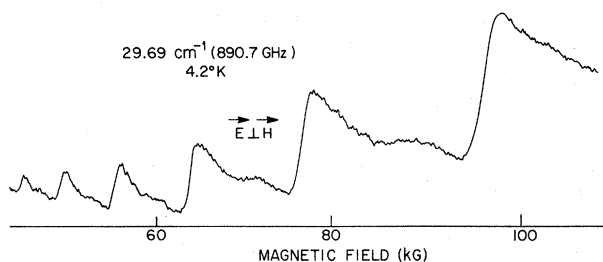


FIG. 7. Real surface impedance versus magnetic field, 4.2°K, 29.69 cm^{-1} , $\vec{E} \perp \vec{H}$.

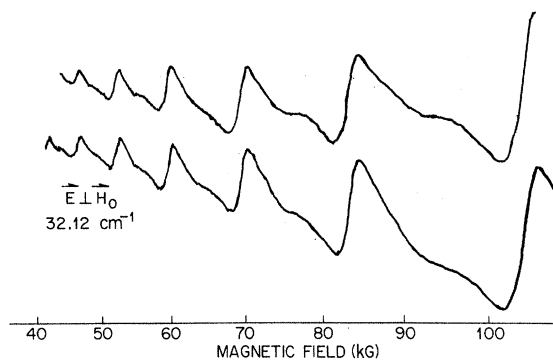


FIG. 8. Real surface impedance versus magnetic field, 4.2°K, 32.12 cm^{-1} , $\vec{E} \perp \vec{H}$.

the retardation regime.³⁹ We also note that, although the $\vec{E} \parallel \vec{H}$ and $\vec{E} \perp \vec{H}$ signals turn on at the same field, the $\vec{E} \perp \vec{H}$ signals show considerably more absorption on the high-field side of cyclotron resonance than do the $\vec{E} \parallel \vec{H}$ signals.

Lastly, we note that a qualitative examination of the data in Figs. 5-10 shows a general broadening of the structure as one goes to higher frequencies. This is due to the increase in quasiparticle relaxation rate, due to electron-phonon coupling, as one increases the frequency of the excitations and approaches the Debye peak in the phonon density of states. This is, of course, the phenomena that we wish to make contact with in a quantitative way. In Sec. IV we examine in detail the cyclotron resonance line shape and position to extract some measure of the electron-phonon contribution to the quasiparticle self-energy.

IV. ANALYSIS

The object of the following analysis is to extract from these far-infrared measurements of cyclotron resonance a spectroscopic measure of the electron-phonon coupling. As Scher and Holstein¹¹ point out, there are two experimental handles on the electron-

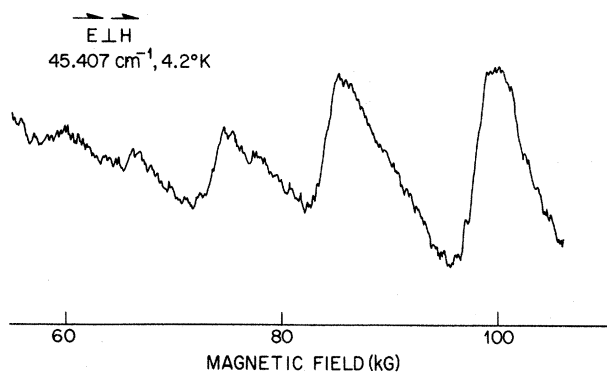


FIG. 9. Real surface impedance versus magnetic field, 4.2°K, 45.407 cm^{-1} , $\vec{E} \perp \vec{H}$, (nine-run average).

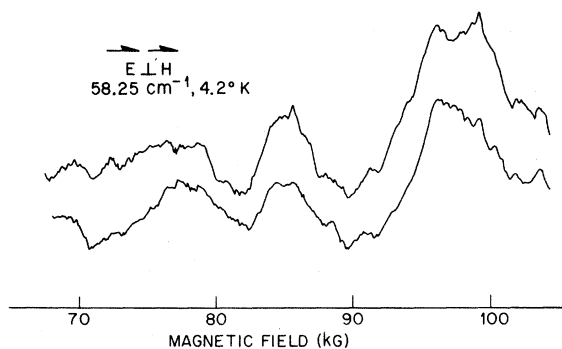


FIG. 10. Real surface impedance versus magnetic field, 4.2 °K, 58.25 cm⁻¹, $\vec{E} \perp \vec{H}$, (nine-run average).

phonon coupling—a shift in effective mass with frequency and a strong increase in relaxation rate. The mass is, of course, determined by the resonance position, whereas the relaxation rate is reflected in the line shape, which, as we shall see, is not particularly well understood. On the other hand, only 0.5% mass changes are expected as compared with a 100-fold increase in relaxation rate. Consequently, despite the uncertainty in line shape, the relaxation rate is probably the most effective measure of the electron-phonon coupling. Indeed, if we were to focus attention on the mass, we would find that 0.1% precision is required to make a meaningful measurement of the frequency dependence of the real part of the electron-phonon self-energy. Such a measurement would be equally sensitive to our understanding of the line shape. As a result, the main thrust of the present analysis is to extract the electron-phonon interaction strength from the relaxation rate or imaginary part of the self-energy.

Although cyclotron resonance in solids is a well-understood physical concept, a precise mathemati-

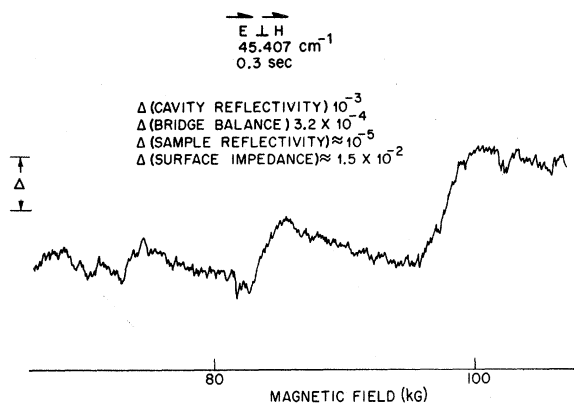


FIG. 11. Real surface impedance versus magnetic field, 4.2 °K, 45.407 cm⁻¹, $\vec{E} \perp \vec{H}$, 0.3-sec time constant.

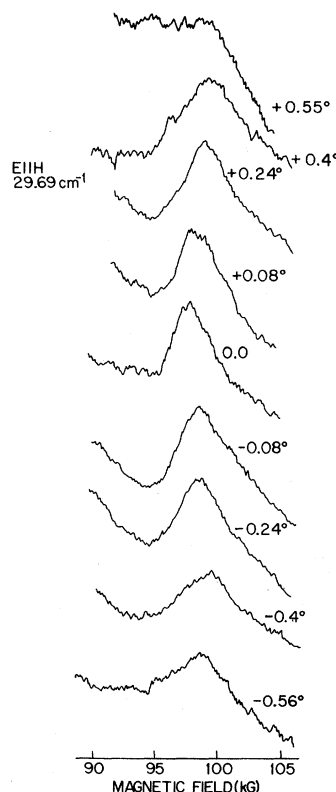


FIG. 12. Tip dependence of the fourth subharmonic for $\vec{E} \parallel \vec{H}$ at 29.69 cm⁻¹.

cal description of the effect, especially in metals where the surface plays a crucial role, is difficult to obtain.⁶⁷ The basic effect as first described by Azbel' and Kaner¹⁰ is shown in Fig. 13. In the presence of a magnetic field parallel to the surface, the electrons execute orbits, some of which just pass through the skin depth. Anomalies in the surface impedance occur whenever the frequency of the incident radiation is an integral multiple of the cyclotron frequency. There are a number of basic lengths and times in the problem which are indicated in the figure, and they are the cyclotron radius R_c , the skin depth δ , the frequency of the incident radiation ω , and the cyclotron frequency ω_c .

The key theoretical treatments of the problem at microwave frequencies are the original work by Azbel' and Kaner,^{10,68} the appropriate modifications by Chambers⁶⁹ to treat small pieces of resonant Fermi surface in a much larger nonresonant background, and the exact treatment of Hartman and Luttinger.⁷⁰ Essential to these treatments is the approximation that the time an electron spends in the skin depth is small compared with the period of the electromagnetic field. The time spent in the skin depth for $R_c \gg \delta$ is approximately

$$T_s = \frac{1}{\omega_c} \left(\frac{2\delta}{R_c} \right)^{1/2}. \quad (7)$$

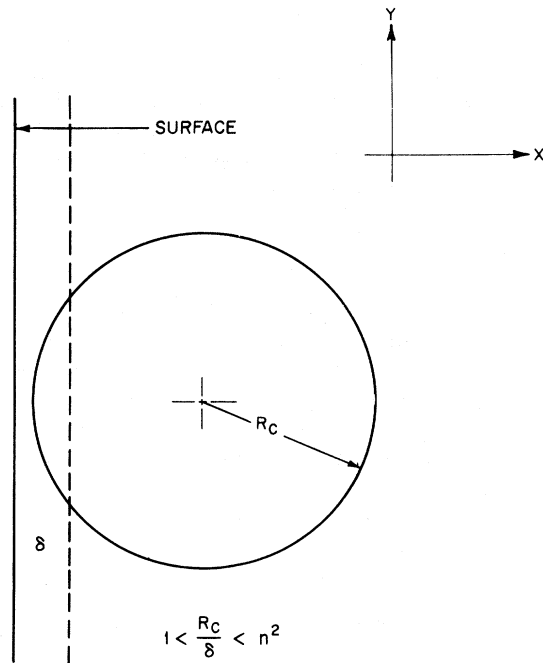


FIG. 13. Length parameters in Azbel'-Kaner cyclotron resonance.

For the usual cyclotron resonance theories to be valid, we must have

$$\omega T_s \ll 1 \quad (8)$$

or

$$\frac{\omega}{\omega_c} \ll \left(\frac{R_c}{2\delta} \right)^{1/2}. \quad (9)$$

This may be expressed another way. If we are observing the n th subharmonic, then $\omega/\omega_c = n$, and we have the condition

$$R_c/\delta \gg 2n^2. \quad (10)$$

In fact, we can resolve three regimes for cyclotron resonance in solids with Eq. (10):

$$R_c/\delta > n^2, \quad (11a)$$

$$n^2 > R_c/\delta > 1, \quad (11b)$$

$$1 > R_c/\delta. \quad (11c)$$

[We ignore the factor of 2 in (10) and note that the crossover from one regime to the other is not well defined.] Equation (11a) is appropriate to microwave frequency Azbel'-Kaner cyclotron resonance in real metals, while (11c) describes cyclotron resonance in semiconductors with low carrier density. Retarded cyclotron resonance, recently discussed by Drew³⁹ and Meierovich,⁴⁰ occurs if R_c/δ satisfies (11b). Most cyclotron resonance experiments in real metals in the far infrared will fall into this category. For instance, consider potas-

sium in a 100-kG field at 29.69 cm^{-1} . $R_c \sim 5000 \text{ \AA}$, $\delta \sim 500 \text{ \AA}$, $\omega/\omega_c = 4$; then $n^2 = 16$ and $R_c/\delta = 10$. In these experiments this is as close as we come to the true Azbel'-Kaner condition (11a), for at higher frequencies or lower fields the ratio $R_c/\delta n^2$ becomes even smaller.

In Fig. 14 we show the Azbel'-Kaner result⁶⁸ for 29.69 cm^{-1} , a mass of $1.217m$, and a relaxation rate of 0.23 cm^{-1} , which are quite close to the final values determined from a better model, only to emphasize the qualitative differences between the Azbel'-Kaner theory, appropriate to microwave frequencies, and the far-infrared results. The essential differences are the following: The calculated change in surface impedance is approximately two orders of magnitude larger than the experimental result. The theoretical resonance is characterized by a rapid rise in real surface impedance rather than the peak seen in the experimental data. The subharmonics are only weakly attenuated by the finite relaxation rate, whereas the subharmonic structure in the experimental traces are rapidly attenuated by the retardation effect. The calculated surface impedance varies smoothly between subharmonics, whereas the experiment shows structure and a marked difference between $\vec{E} \parallel \vec{H}$ and $\vec{E} \perp \vec{H}$.

The mathematical model used to analyze the data is an extension of the approach taken by Drew³⁹ to describe retarded cyclotron resonance. One starts with the variational form of the surface admittance Y , first formulated by Marcus⁷¹ and subsequently used by a number of authors dealing with the sur-

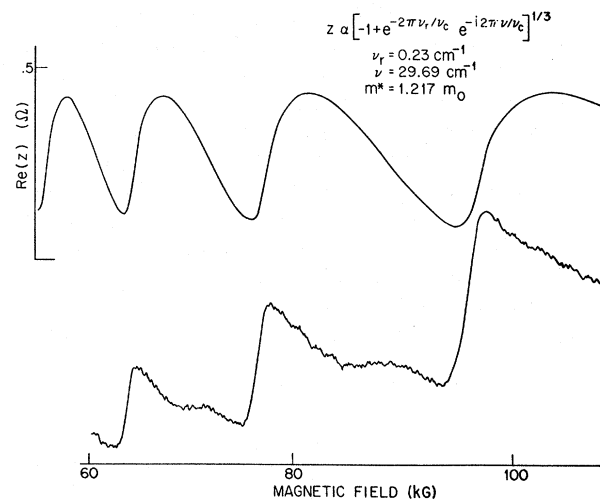


FIG. 14. Real surface impedance versus magnetic field for cyclotron resonance in the Azbel'-Kaner limit (upper part). In bottom part, we show the experimental result for $\vec{E} \perp \vec{H}$. The ordinate is not precisely determined but is estimated to be 10^{-2} of the ordinate scale in the upper figure.

face impedance of a metal^{39,72-74}:

$$i\omega\mu_0 Y = \int_0^\infty dx E_y'(x)^2 + E_z'(x)^2 + i\omega\mu_0 \int_0^\infty dx [J_y(x)E_y(x) + J_z(x)E_z(x) - J_x(x)E_x(x)], \quad (12)$$

where z is taken as the magnetic field direction and x the normal to the surface (see Fig. 13). $\vec{E}(x)$ is the infrared electric field, normalized to unity at $x=0$, the surface of the metal, and $\vec{J}(x)$ is the infrared currents produced by the electric field:

$$\vec{J}(x) = \int_0^\infty dx' \vec{\sigma}(x, x') \cdot \vec{E}(x'). \quad (13)$$

If it can be correctly assumed that on resonance the change in electric field is small, then, to first order in the change in nonlocal conductivity $\delta\vec{\sigma}(x, x')$, the change in admittance is⁷²

$$\delta Y = \int_0^\infty dx \int_0^\infty dx' \vec{E}(x) \cdot \delta\vec{\sigma}(x, x') \cdot \vec{E}(x'), \quad (14)$$

where one uses the electric field off resonance, or the electric fields at $H=0$, to evaluate (14).

Drew³⁹ used (14) to discuss retardation effects in situations where the number of resonant electrons is a small fraction of the total number of electrons. Under these conditions, the assumption of small changes in the electric field can be satisfied. At first sight, the approximation—that the fields in potassium are not changed much near resonance—seems absurd, since all the electrons in the bulk in potassium resonate at the same frequency. However, it proves to be the case that in the skin depth, where most of the electrons strike the surface, and therefore are nonresonant, and in the retardation regime, where $V_F/\omega \lesssim \delta$, the field changes are small. Anticipating our results, however, we note that (14) fails to account for all the aspects of cyclotron resonance in potassium in the far infrared, and these departures from (14) appear to be due to a failure of this approximation not at the surface but in the bulk. That is to say, the fractional changes in electric field are small at the surface but large in the bulk. We make these remarks here to emphasize that (14) should not be dismissed out of hand and indeed provides a good first approximation to the solution as well as a starting point for

more exact treatments.

The approximate solution found by Drew³⁹ for a cylindrical Fermi surface is clearly inappropriate to potassium. However, Eq. (14) can be integrated exactly for exponential fields and a spherical Fermi surface. This is done in Appendix A, and we simply quote the result here:

$$\delta Y = \frac{Ne^2}{m\omega_c} \sum_{n=-\infty}^{+\infty} \frac{A_n(\alpha, R_c)}{i(\omega/\omega_c + n)}, \quad (15)$$

where N is the electron density, e the electron charge, m the clothed mass, and ω_c the cyclotron frequency $\omega_c = eB/m$. In (15) we have assumed a constant mass and infinite relaxation time. $A_n(\alpha, R_c)$ determines the strength of the resonance at the n th subharmonic and describes the retardation effects. $A_n(\alpha, R_c)$ depends on polarization of the radiation, and we obtain for $\vec{E} \parallel \vec{H}$

$$A_n^{zz}(\alpha, R_c) = (3/4\alpha) \int_0^\pi d\theta \times \sin\theta \cos^2\theta e^{-2\alpha R} J_n(-i\alpha R) J_n(i\alpha R), \quad (16)$$

where $R = R_c \sin\theta$, J_n is the n th-order Bessel function of the first kind with complex argument, and α describes the complex decay of the infrared electric field $E = e^{-\alpha x}$. For $\vec{E} \perp \vec{H}$ we obtain

$$A_n^{yy}(\alpha, R_c) = (3/4\alpha) \int_0^\pi d\theta \times \sin^3\theta e^{-2\alpha R} J_n'(-i\alpha R) J_n'(i\alpha R), \quad (17)$$

where J_n' is the derivative of the n th-order Bessel function. Equation (15), then, describes a sum of Lorentzians weighted by a complex retardation parameter (16) or (17), which depends on the polarization of the incident radiation.

The electron-phonon effects are introduced following Scher and Holstein,¹¹ who find that correct to order δ/R_c , one need only replace the denominator of the Lorentzian in (15) with an average of Lorentzians for all possible particle-hole pairs that can be created near the Fermi surface by radiation of energy $\hbar\omega$. The Lorentzian for a particular electron-hole pair will be shifted and broadened by the electron-phonon contribution to the quasiparticle self-energy depending on the position of the particle-hole pair with respect to the Fermi energy. In particular,

$$\frac{1}{i(\omega/\omega_c + n)} \rightarrow \int_{-\infty}^{+\infty} \frac{dE}{\hbar\omega} [f(E) - f(E + \hbar\omega)] \left\{ i \left[\frac{\omega}{\omega_c} \left(1 + \frac{M(E) - M(E + \hbar\omega)}{\hbar\omega} \right) + n \right] + \frac{\Gamma(E) + \Gamma(E + \hbar\omega)}{\hbar\omega_c} \right\}^{-1}, \quad (18)$$

where $M(E)$ and $\Gamma(E)$ are the real and imaginary parts of the quasiparticle self-energy at an energy E above or below the Fermi energy. ω_c is now the bare mass (less electron-phonon effects but still

dressed by electron-electron interactions). f is the Fermi function. f , M , and Γ are all implicit functions of temperature. We are clearly ignoring any anisotropy in the self-energy due to the phonon

anisotropy.³²

We obtain then the following expression for the change in admittance on resonance:

$$\delta Y = \frac{Ne^2}{m\omega_c} \sum_{n=-\infty}^{+\infty} A_n(\alpha, R_c) \int \frac{dE}{\hbar\omega} \frac{f(E) - f(E + \hbar\omega)}{\gamma(E) + in}, \quad (19)$$

where

$$\gamma(E) = i \frac{\omega}{\omega_c} \left(1 + \frac{M(E) - M(E + \hbar\omega)}{\hbar\omega} \right) + \frac{\Gamma(E) + \Gamma(E + \hbar\omega)}{\hbar\omega_c}. \quad (20)$$

To obtain $M(E)$ and $\Gamma(E)$ we use the following expressions^{7,11,13,14}:

$$M(E) = \int dE' \int_0^\infty d\omega \alpha^2 F(\omega) \times \left(\frac{1 - f(E') + N(\hbar\omega)}{E - E' - \hbar\omega} + \frac{f(E') + N(\hbar\omega)}{E - E' + \hbar\omega} \right) \quad (21)$$

and

$$\Gamma(E) = \pi \int_0^\infty d\omega \alpha^2 F(\omega) [1 - f(E - \hbar\omega) + N(\hbar\omega) + f(E + \hbar\omega) + N(\hbar\omega)], \quad (22)$$

where f and N are the Fermi and Bose occupation factors. $\pi\alpha^2 F(\omega)$ gives the scattering rate for a quasiparticle accompanied by the emission of a phonon of energy $\hbar\omega$. It includes both the density of phonon states and a matrix element squared and in this approximation excludes any possible k dependence of the scattering. The Fermi and Bose occupation factors ensure that we scatter to an unoccupied state and that at finite temperatures we can absorb as well as emit phonons at a rate that depends on the number of phonons in the field.

All that is needed to calculate the real and imaginary parts of the self-energy is $\alpha^2 F(\omega)$, which we take from the work of Dynes and Carbotte²⁵ and Carbotte, Dynes, and Trofimenkoff.²⁶ Their $\alpha^2 F(\omega)$ is calculated from the Heine-Abarenkov pseudopotential⁷⁵⁻⁷⁷ and a model for the phonons given by a Born-von Karman fit to the phonon dispersion relations determined from neutron scattering.⁷⁸ $\alpha^2 F$ is sensitive to choice of pseudopotential but restricting pseudopotential to those that give reasonable fits to resistivity versus temperature, one finds only 20% variations. An unambiguous determination of $\alpha^2 F$ from high-frequency cyclotron resonance is not a possibility at present. The $\alpha^2 F$ used in the present calculations is shown in Fig. 15.

A convenient measure of the strength of the interaction is the electron-phonon λ which determines the low-frequency $T=0^\circ\text{K}$ mass

$$m^* = (1 + \lambda) m_b \quad (23)$$

and is related to $\alpha^2 F(\omega)$ by

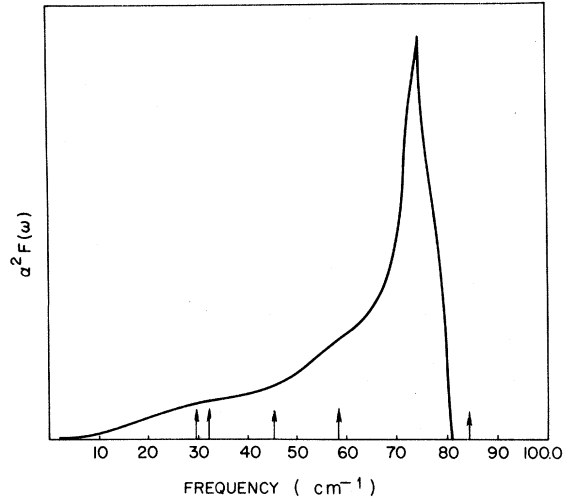


FIG. 15. $\alpha^2 F(\omega)$ from Refs. 25 and 26. Arrows indicate laser frequencies for this experiment.

$$\lambda = 2 \int_0^\infty \frac{d\omega}{\omega} \alpha^2 F(\omega). \quad (24)$$

Carbotte *et al.* calculated λ to be 0.107.^{25,26} In the following we leave the shape of $\alpha^2 F(\omega)$ fixed but let the strength of the coupling vary and attempt to determine a scale factor or λ by comparison of the model calculation, with adjustable λ , to experiment.

We note that the dc mass in (23) is accurately determined, by the work of Walsh,³⁷ to be $(1.217 \pm 0.002)m$ so that for a given λ we introduce a bare mass given by $m_b = 1.217m/(1 + \lambda)$. In effect then we have only one model parameter to adjust, viz., λ , which adjusts the over-all strength of the electron-phonon coupling.

To summarize the results of this model calculation, we refer again to Eqs. (19)–(24). The change in admittance is given by a sum of Lorentzians broadened and shifted by the electron-phonon interaction whose strength is given by λ . Each Lorentzian, corresponding to absorption at a particular subharmonic, is weighted by a complex factor $A_n(\alpha, R_c)$ that depends on polarization with respect to the magnetic field and describes the effect of retardation on the subharmonic resonance. The nonadjustable parameters in the model calculation are the zero frequency mass, the electron density, and the shape but not the magnitude of $\alpha^2 F$. The magnitude of $\alpha^2 F$ is left adjustable and is given by λ .

The results of such a calculation for $\vec{E} \parallel \vec{H}$ and $\vec{E} \perp \vec{H}$ for a $\lambda = 0.1$ are shown in Figs. 16 and 17. It appears that the model calculation properly describes the turn on of cyclotron resonance, for increasing magnetic field, and the attenuation of the

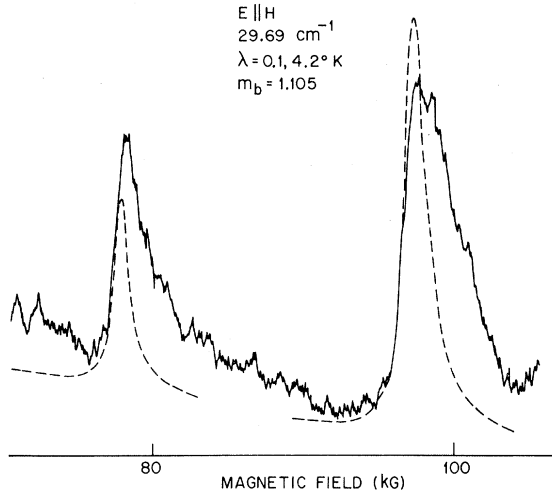


FIG. 16. Calculated and experimental traces of real surface impedance versus magnetic field for $\vec{E} \parallel \vec{H}$, 29.69 cm^{-1} , 4.2°K assuming $\lambda=0.1$. No attempt is made to determine the absolute scale for the experimental plot. The dashed lines are not connected since we wished to correct for the experimental background drift by simply plotting the resonance region calculated for each subharmonic individually in close proximity to the experimental curve. The scale for the two theoretical plots is the same.

subharmonic resonances. (In fact, for $\vec{E} \parallel \vec{H}$ the subharmonic resonances experimentally drop off at a rate which is approximately 20% less than that calculated.) However, the model fails to account for the absorption on the high-field side of cyclotron resonance. This is especially so for the case of $\vec{E} \perp \vec{H}$. No reasonable amount of distortion of these basic Lorentzians by increased relaxation rate or increased retardation parameter αR_c will

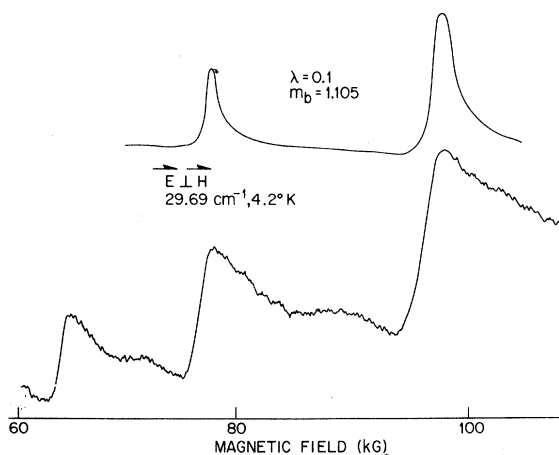


FIG. 17. Calculated and experimental traces of real surface impedance versus magnetic field for $\vec{E} \perp \vec{H}$, 29.69 cm^{-1} , 4.2°K assuming $\lambda=0.1$.

reproduce the absorption or structure on the high-field side.

In Figs. 18 and 19 we compare the experimental data with the infinite medium dispersion relations for real electromagnetic wave propagation across the magnetic field. That such wave propagation does occur has been clearly demonstrated at microwave frequencies by Walsh and Platzman³⁻⁵ and co-workers.^{79,80} The infinite medium dispersion relations are obtained from^{5,81}

$$k^2 = i\omega\mu_0\sigma_{zz}(k, \omega), \quad \vec{E} \parallel \vec{H} \quad (25)$$

$$= i\omega\mu_0\left(\sigma_{yy}(k, \omega) + \frac{\sigma_{xy}(k, \omega)^2}{\sigma_{xx}(k, \omega)}\right), \quad \vec{E} \perp \vec{H}. \quad (26)$$

Equations (25) and (26) were solved on a computer⁸² assuming infinite $\omega\tau$ and a mass of $1.21m$ in the case of $\vec{E} \perp \vec{H}$ at 32.12 cm^{-1} and a mass of $1.217m$ for $\vec{E} \parallel \vec{H}$ at 29.69 cm^{-1} . (The reader should disregard the small difference in the masses used for the two calculations. The difference is unimportant for the present discussion.)

An inspection of Figs. 18 and 19 shows that the high-field cutoff of the absorption for $\vec{E} \parallel \vec{H}$ and the high-field structure indicated by the changing slope of the absorption versus field for $\vec{E} \perp \vec{H}$ correlate with the extremal points in the infinite medium dispersion relations. It is quite clear that the model calculation given by Eq. (14) is not sensitive to the bulk properties and cannot give structure on

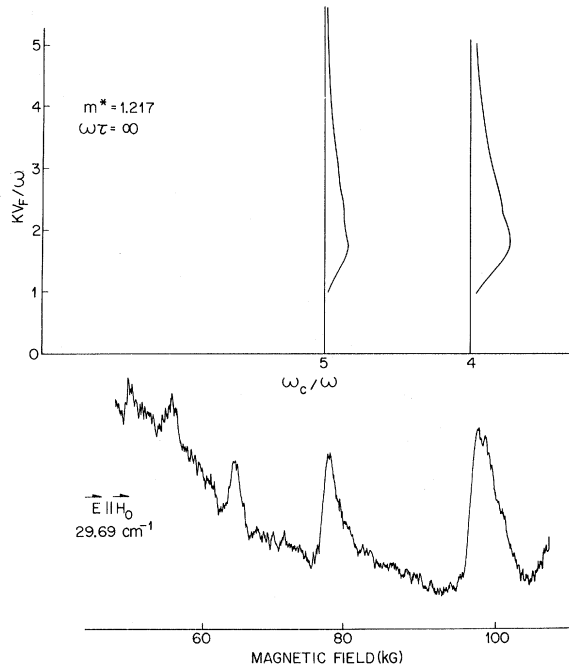


FIG. 18. Real surface impedance versus magnetic field $\vec{E} \parallel \vec{H}$, 29.69 cm^{-1} , 4.2°K compared with infinite medium dispersion relations for cyclotron waves assuming $m^*=1.217$ and $\omega\tau=\infty$.

the high-field side associated with these waves. The resonances in the model calculation are due to *surface currents* only.

At this point one may be inclined to go to the other extreme and ignore the surface altogether. If the surface is unimportant, one may use the pseudospecular boundary condition⁶⁷ and obtain for the surface impedance Z

$$Z = \frac{i\omega\mu_0}{\pi} \int_{-\infty}^{+\infty} \frac{dk}{k^2 + i\omega\mu_0\sigma_{zz}(k, \omega)}. \quad (27)$$

Performing such an integration, we obtain the results shown in Fig. 20 for $\vec{E} \parallel \vec{H}$ at 29.69 cm^{-1} for $\lambda = 0.1$. As expected, the results emphasize the wave aspects rather than the resonances in quasiparticle surface currents. The absorption line shape mirrors the density of wave states that can be excited and peaks near the point where $|d\omega/dk| \approx 0$.⁸³ This solution is valid⁴⁰ only for $R_c < \delta$, which is clearly not satisfied in K for available magnetic fields. It appears then that the proper theory will combine the solution given in (19), which describes the resonances in the single quasiparticle currents near the surface, with a solution of the form (27) which describes the excitation of waves in the bulk. Such a solution does not exist at present so that a detail fit to the experimental line shapes is not

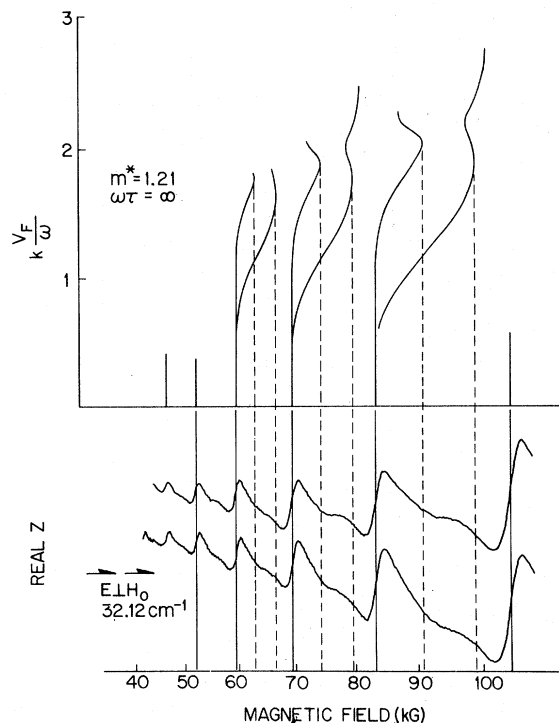


FIG. 19. Real surface impedance versus magnetic field $\vec{E} \perp \vec{H}$, 32.12 cm^{-1} , 4.2°K compared with infinite medium dispersion relations for cyclotron waves assuming $m^* = 1.21$ and $\omega\tau = \infty$.

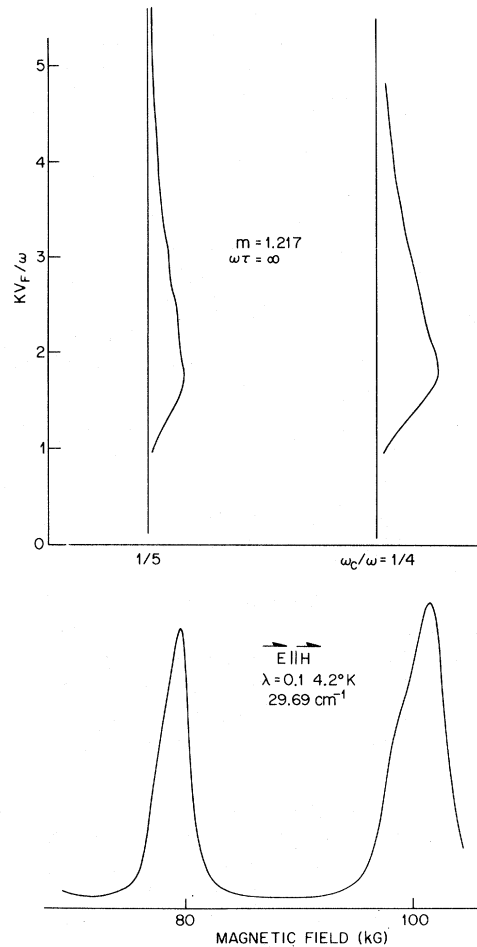


FIG. 20. Surface impedance versus magnetic field calculated from Eq. (27), which assumes pseudospecular boundary condition.

possible.

Nevertheless we can proceed in a somewhat heuristic vein. In particular, we question under what circumstances (19) should be valid. It seems clear that the solution fails because we can excite waves in the bulk. This implies that our initial assumption—that the electric fields were only weakly modified on resonance—does not hold in the bulk, despite the fact that it does hold near the surface. Clearly then, metals in which wave propagation is inhibited should still be amenable to Drew's analysis in quantitative detail. This condition is achieved by allowing a strong nonresonant background conductivity which has the effect, in Eqs. (25) and (26) for the infinite medium dispersion relations, of reducing the dispersion of the waves. In particular, for arbitrarily large nonresonant background, the cyclotron resonance can overcome the conduction losses only very close to cyclotron resonance allowing wave propagation in an arbitrarily narrow window near cyclotron reso-

nance. Stated another way, ω versus k for the cyclotron waves becomes a straight line at the subharmonic resonance $\omega = n\omega_c$, the group velocity $\partial\omega/\partial k$ is zero, and no energy is carried into the bulk. Under these circumstances, cyclotron resonance should be characterized by (19). (At microwave frequencies we would describe such a resonance by the Chambers theory⁶⁹ with $a \gg 1$.)

The above discussion suggests that Eq. (19) may, in fact, still contain some elements of truth even for potassium if we restrict our discussion to regions where there is no wave propagation or where the group velocity is zero for an extended range of wave vectors. This occurs at cyclotron resonance itself, where the dispersion relations asymptotically approach $\omega = \omega_c$ for large k .⁶⁴ At this point energy is not carried into the bulk, and the change in surface admittance should be dominated by resonances in single quasiparticle currents at the surface. Furthermore, for $\vec{E} \parallel \vec{H}$ the metal propagates no waves immediately below cyclotron resonance and therefore the line shape should be least encumbered by wave effects near cyclotron resonance for this polarization. This does not appear to be true for $\vec{E} \perp \vec{H}$, where longitudinal wave propagation can occur just below resonance (see Fig. 19).

In summary then, we argue that the variational approach that results in Eq. (19) and describes the change in surface impedance in terms of resonances in the quasiparticle currents excited in the skin depth may adequately describe the onset of cyclotron resonance for $\vec{E} \parallel \vec{H}$ for the following reasons. (1) At least for $\vec{E} \parallel \vec{H}$ no waves propagate across the field for magnetic fields just below the resonant field. (2) The waves that may propagate at cyclotron resonance have vanishing small group velocity and carry no energy into the bulk, minimizing bulk effects. (3) The waves that are excited at cyclotron resonance have large k vectors and the large k vector solution to Maxwell's equations should be dominated by the resonances in the single quasiparticle currents [this may be a restatement of (2)]. (4) It seems to work. The last reason clearly carries the most weight.

Assuming that this hypothesis is correct, we measure the strength of the electron-phonon interaction, as given by λ in the model calculation, by matching the normalized slope of the onset of cyclotron resonance in the experiment to the theory. By normalized slope we mean $\partial \text{Re}(Z)/\partial H$ half-way up the leading edge divided by $\Delta \text{Re}(Z)$, the total change in surface impedance at resonance. Table I gives the values of λ that one obtains, and it can be seen that despite the scatter, they are consistent with a λ of 0.11 ± 0.02 . This agrees quite well with the value deduced from the temperature-dependent resistivity.²⁵⁻³¹ Although a single relaxa-

TABLE I. Electron-phonon λ .

	$n=4$	$n=5$
29.69 cm ⁻¹	0.11	0.114
32.12 cm ⁻¹	0.127	0.099

tion rate is not appropriate to electronic excitations at this frequency [the relaxation parameter $\Gamma(E) + \Gamma(E + \hbar\omega)$ in Eq. (20) varies by about a factor of 3 depending on the position E with respect to the Fermi surface], we can define an average rate

$$\frac{\hbar}{\tau} = \left[\int \frac{dE}{\hbar\omega} \frac{f(E) - f(E + \hbar\omega)}{\Gamma(E) + \Gamma(E + \hbar\omega)} \right]^{-1}$$

and this corresponds to $\approx 0.23 \text{ cm}^{-1}$ at 29.69 cm^{-1} .

We pursue this approach to the problem a little further and recompute the absorption line shape assuming $\lambda = 0$ but that we have a constant relaxation rate of 0.23 cm^{-1} and a mass of $1.217m$. The results are shown in Fig. 21. The edge is clearly shifted to lower fields by about 1 kG. The uncertainty in calculated position from the magnetic field calibration and the uncertainty in the microwave mass is $\pm 300 \text{ G}$. This indicates that the determined λ and model calculation account for *both* the edge position and breadth.

We have not pursued this analysis for $\vec{E} \perp \vec{H}$, since it is clear from the experimental data that wave propagation associated with the longitudinal mode is contributing to absorption on the low-field side of resonance quite close to the resonance field. We have, however, calculated the line shape from (19) with $\lambda = 0.1$ and compare with experiment in Figs. 17 and 22-24. It can be seen that the correct peak position is obtained, but the experimental breadth of the leading edge exceeds that calculated by $\sim 50\%$, which may be due to the wave aspects on the low-field side that are not properly included in the calculation. Consistently the absorption on the high-field side of cyclotron resonance in the experimental traces is stronger than calculated. We note that the average scattering rate at 58.25 cm^{-1} (Fig. 24) for $\lambda = 0.1$, is about 1.2 cm^{-1} , about a six-fold increase over the solution for 29.69 cm^{-1} and gives a $\omega_c\tau$ of about 6 at the eighth subharmonic.

V. CONCLUSIONS

The electron-phonon λ of 0.11 ± 0.02 determined from the position and breadth of the leading edge of the $\vec{E} \parallel \vec{H}$ cyclotron resonance agrees quite well with previous experimental and theoretical estimates of λ . As we have noted earlier, the temperature-dependent resistivity²⁷⁻²⁹ in pure potassium can be used to deduce the electron-phonon coupling. The basic approach is to fit the temperature-dependent resistivity by using a variety of pseudopotentials or, in some cases, a pseudopotential with adjustable

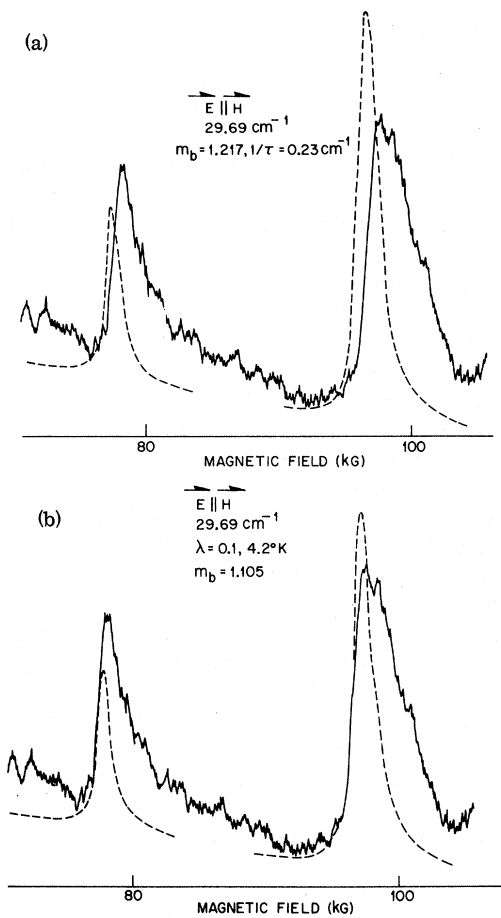


FIG. 21. (a) Calculated line shape and position assuming $\lambda=0$ and $m_b=1.217m$ but $1/\tau=0.23\text{ cm}^{-1}$. (b) Calculated line shape and position assuming $\lambda=0.1$ and a bare mass of 1.105.

parameter. The pseudopotential thus determined can be used to calculate an $\alpha^2 F(\omega)$ which is the basic input to the present experiments. Such fits have been performed by Dynes and Carbotte,²⁵ Ekin,²⁸ Ekin and Maxfield,²⁹ Hayman and Carbotte,³⁰ and Rice and Sham.³¹ While the resistivity versus temperature is a very sensitive function of pseudopotential,²⁹ the value of λ is not. Nonetheless, since there is ambiguity in determining the appropriate pseudopotential from phonon-limited resistivity, there is some ambiguity in λ . It is, perhaps, instructive to consider the following cases. Ekin and Maxfield²⁹ fit the phonon-limited resistivity from 1 to 25 °K by adjusting the core radius of an Ashcroft pseudopotential⁸⁵ and obtain a radius which agrees quite well with that determined from a Fermi-surface fit.⁸⁵ The latter pseudopotential as treated by Rice³² gives a value for λ of 0.12. On the other hand, Hayman and Carbotte³⁰ fit the resistivity over a wider range with a core radius 10% less and subsequently Leavens and Carbotte³³

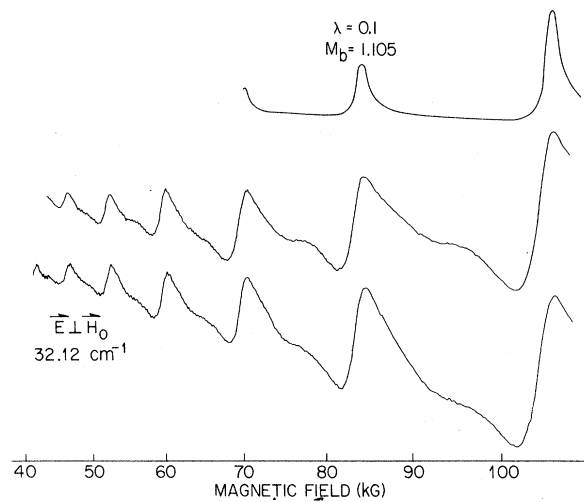


FIG. 22. Calculated real surface impedance $\vec{E} \perp \vec{H}$, 32.12 cm^{-1} , $4.2\text{ }^\circ\text{K}$, $\lambda=0.1$ compared with experiment.

calculate a λ of 0.13. A λ of 0.11 is obtained by Carbotte, Dynes, and Trofimenkoff²⁶ using a Heine-Abarenkov pseudopotential used to obtain resistivity versus temperature in potassium over a narrower temperature range.²⁵ There are a number of other calculations of λ ,³⁴ starting with pseudopotentials that fit some other parameter, say the shape of the Fermi surface, and are not, therefore, required to directly reproduce some aspect of the electron-phonon scattering. Such a sample of calculations gives a spread in theoretical values for λ from 0.1 to 0.18, but if we restrict our attention to pseudopotentials that fit the phonon-limited resistivity, then one obtains a value of λ with considerably less spread, 0.11–0.13.

The agreement obtained between the λ determined from high-frequency cyclotron resonance and phonon-limited resistivity may very well be

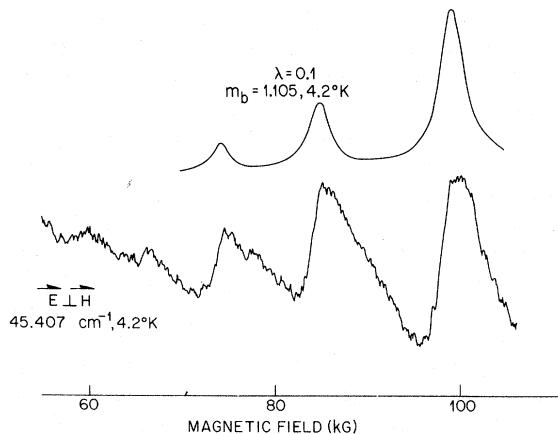


FIG. 23. Calculated real surface impedance $\vec{E} \perp \vec{H}$, 45.407 cm^{-1} , $4.2\text{ }^\circ\text{K}$, $\lambda=0.1$ compared with experiment.

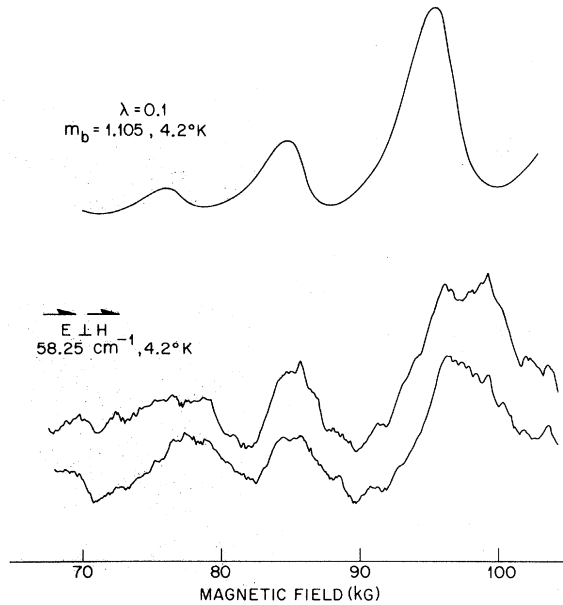


FIG. 24. Calculated real surface impedance $\bar{E} \perp \bar{H}$, 58.25 cm^{-1} , 4.2°K , $\lambda = 0.1$ compared with experiment.

fortuitous. As previously discussed, two effects enter the phenomenon of cyclotron resonance as one extends the operating frequency into the far infrared. The first is a self-energy correction due to the electron-phonon scattering; the second is the change in the electrodynamic introduced by retardation effects. It seems quite clear at this point in time that the latter is less well understood than the former. Since no exact solution to the surface impedance problem exists, one cannot help but have serious reservations as to whether an approximate treatment of the retardation problem which reproduces only some of the features can be used to extract the electron-phonon contributions to the line shape. Viewed in this light, perhaps the success of the fit of the variational solution to the leading edge of cyclotron resonance, for $\bar{E} \parallel \bar{H}$, for a reasonable λ , confirms our solution of Maxwell's equation near cyclotron resonance rather than our choice of λ .

Some other remarks are in order with regard to how effective high-frequency cyclotron resonance will be in probing the electron-phonon contribution to the self-energy. It is clear that although one uses monochromatic radiation, the electromagnetic probe is not a narrow-band probe of the self-energy correction. In particular, the electron-hole pairs that contribute to the conductivity average the real and imaginary parts of the self-energy from zero energy to $\hbar\omega$. This is to be contrasted with the tunneling probe which is intrinsically, if not practically, a monochromatic probe. Fine structure then is not to be resolved with the electromagnetic

probe, but only the general strength of the interaction and a general confirmation of a theoretically provided $\alpha^2 F$. (The shape of $\alpha^2 F$ could in principle be deduced if continuous measurements could be made as a function of frequency.) Cyclotron resonance is, however, specified to an orbit on the Fermi surface so that it can give an orbital resolution of the Fermi surface, which the tunneling experiment generally cannot. Indeed, this may be a source of the discrepancy, reported by Goy *et al.*,¹⁹ between the frequency dependence of the mass and lifetime in Pb, and that predicted from the tunneling data. It would seem, then, that the cyclotron resonance probe of the frequency dependence of the electron-phonon self-energy would be most effective in normal metals, which are inaccessible to tunneling experiments, to confirm the general shape of $\alpha^2 F(\omega)$ and measure the over-all strength of the electron-phonon coupling, or to make orbit specific measurements of the electron-phonon relaxation rate in any metal. We emphasize again, however, that an unambiguous interpretation of these experiments requires a reexamination of the problem of Azbel'-Kaner cyclotron resonance in the retardation region. Without a good quantitative theory of cyclotron resonance in this frequency regime, clear interpretation of these experiments cannot be had.

ACKNOWLEDGMENTS

We would like to acknowledge the useful suggestions and criticisms provided by W. M. Walsh, G. A. Baraff, P. M. Platzman, C. C. Grimes, T. M. Rice, R. C. Dynes, and P. B. Allen. M. A. Pollack provided invaluable advice on operating the far-infrared laser. The technical assistance of F. DeRosa is gratefully acknowledged.

APPENDIX A: RESONANT CHANGE IN SURFACE ADMITTANCE

We wish to evaluate Eq. (14) for the resonant change in surface admittance

$$\delta Y = \int_0^\infty dx \int_0^\infty dx' \bar{E}(x) \cdot \delta \bar{\sigma}(x, x') \cdot \bar{E}(x'), \quad (\text{A1})$$

where we assume that the electric field $\bar{E}(x)$ is exponential,

$$\bar{E}(x) = \bar{E}_0 e^{-\alpha x}, \quad (\text{A2})$$

where α is a complex constant. We shall explicitly evaluate (A1) for $\bar{E}(x) \parallel \hat{z}$, the magnetic field direction in Fig. 25. Appropriate to potassium, we assume a spherical Fermi surface with constant mass and solve the Boltzmann equation in the relaxation time approximation. [The modification of the final result due to the electron-phonon self-energy is introduced in the text, Eq. (18).]

We assume that the resonant part of (A1) can be generated by finding the conductivity $\sigma_r(x, x')$ caused by all electrons that do not collide with the

surface. The geometry describing this condition is shown in Fig. 26. We use the formulation of Jones and Sondheimer.⁷³ The real-space orbit radius depends on the zenith angle θ with respect to the magnetic field direction,

$$R(\theta) = R_c \sin \theta. \quad (\text{A3})$$

The belly orbit corresponds to $\theta = \frac{1}{2}\pi$. φ describes the azimuthal position on the orbit. $\varphi = 0$ corresponds to a velocity in the y direction.

If an electron is a distance x from the surface, then it will not collide with the surface, only if it is on a real-space orbit described by θ and φ , at x , such that

$$|\varphi| < 2 \sin^{-1} \left(\frac{x \omega_c}{2v \sin \theta} \right)^{1/2} \quad (\text{A4})$$

or

$$|\varphi| < 2 \sin^{-1} \left(\frac{x}{2R(\theta)} \right)^{1/2}, \quad (\text{A5})$$

where φ spans $-\pi$ to π . If $x > 2R(\theta)$, then there are no bounds on φ .

Following Jones and Sondheimer,⁷³ we write for (A1)

$$\begin{aligned} \delta Y = & \frac{3}{4\pi} \frac{Ne^2}{m\omega_c} \int_0^\infty dx e^{-\alpha x} \int_0^\pi d\theta \sin \theta \cos^2 \theta \int_{-\varphi_m}^{\varphi_m} d\varphi \\ & \times \frac{1}{e^{2\pi\gamma} - 1} \int_\varphi^{\varphi+2\pi} d\varphi' e^{\gamma(\varphi' - \varphi)} e^{-\alpha x - \alpha R(\theta)(\cos \varphi - \cos \varphi')}, \end{aligned} \quad (\text{A6})$$

where N is the electron density, m is the mass, ω_c is the cyclotron frequency, and γ is a complex constant given by

$$\gamma = i \frac{\omega}{\omega_c} + \frac{1}{\omega_c \tau}. \quad (\text{A7})$$

τ is a relaxation rate for the electron gas. φ_m is the limit defined in (A4) and (A5), namely,

$$\varphi_m = 2 \sin^{-1} \left(\frac{x}{2R(\theta)} \right)^{1/2}, \quad x \leq 2R(\theta) \quad (\text{A8})$$

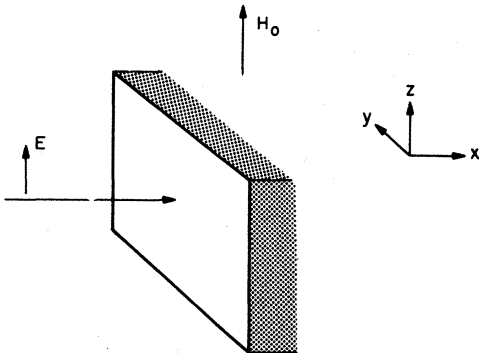


FIG. 25. Specification of coordinate axes relative to sample surface and magnetic field.

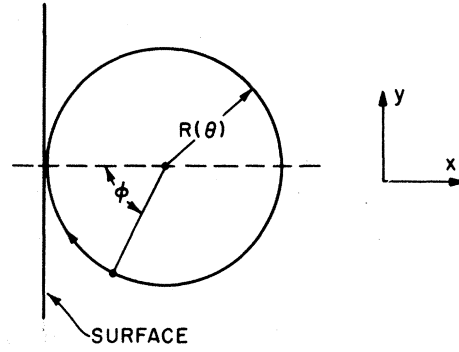


FIG. 26. Orbital parameters used in Eq. (A4).

$$= \pi, \quad x \geq 2R(\theta). \quad (\text{A9})$$

First we rewrite (A6) as

$$\begin{aligned} \delta Y = & \frac{3}{4\pi} \frac{Ne^2}{m\omega_c} \int_0^\pi d\theta \sin \theta \cos^2 \theta \int_0^\infty dx e^{-2\alpha x} \\ & \times \int_{-\varphi_m}^{\varphi_m} d\varphi e^{-\gamma\varphi - \alpha R(\theta) \cos \varphi} \\ & \times \frac{1}{e^{2\pi\gamma} - 1} \int_\varphi^{\varphi+2\pi} d\varphi' e^{\gamma\varphi' + \alpha R(\theta) \cos \varphi'}. \end{aligned} \quad (\text{A10})$$

The φ' integration is performed with the aid of Bessel functions⁸⁶

$$\begin{aligned} \frac{1}{e^{2\pi\gamma} - 1} \int_\varphi^{\varphi+2\pi} d\varphi' e^{\gamma\varphi' + \alpha R(\theta) \cos \varphi'} \\ = \sum_{n=-\infty}^{+\infty} e^{i n \varphi + \gamma \varphi} \frac{J_n(-i\alpha R(\theta))}{(\gamma + in)} e^{i n \pi / 2}, \end{aligned} \quad (\text{A11})$$

where J_n is the n th-order Bessel function of the first kind. Likewise, the φ integration becomes

$$\begin{aligned} \int_{-\varphi_m}^{\varphi_m} d\varphi e^{i n \varphi} e^{-\alpha R(\theta) \cos \varphi} \\ = \sum_l J_l(i\alpha R(\theta)) e^{i l \pi / 2} \frac{2 \sin(l+n)\varphi_m}{l+n}. \end{aligned} \quad (\text{A12})$$

Then (A10) is rewritten

$$\begin{aligned} \delta Y = & \frac{3}{4\pi} \frac{Ne^2}{m\omega_c} \int_0^\pi d\theta \sin \theta \cos^2 \theta \int_0^\infty dx e^{-2\alpha x} \\ & \times \sum_{n=-\infty}^{+\infty} \sum_{l=-\infty}^{+\infty} e^{i(n+l)\pi/2} \frac{J_l(i\alpha R(\theta)) J_n(-i\alpha R(\theta))}{\gamma + in} \\ & \times \frac{2 \sin(l+n)\varphi_m}{l+n}, \end{aligned} \quad (\text{A13})$$

where we note that φ_m is a function of x given in (A8) and (A9).

We next evaluate

$$\int_0^\infty dx e^{-2\alpha x} \frac{\sin(l+n)\varphi_m}{l+n}$$

$$= \int_0^{2R(\theta)} dx e^{-2\alpha x} \frac{\sin\{2(l+n)\sin^{-1}[x/2R(\theta)]^{1/2}\}}{l+n},$$

$$l+n \neq 0$$

$$= \int_0^{2R(\theta)} dx e^{-2\alpha x} 2 \sin^{-1}\left(\frac{x}{2R(\theta)}\right)^{1/2} + \pi \int_{2R(\theta)}^{\infty} dx e^{-2\alpha x},$$

$$l+n = 0. \quad (\text{A14})$$

Consider first the case of $l+n \neq 0$. We substitute

$$y = \left(\frac{x}{2R(\theta)}\right)^{1/2} \quad (\text{A15})$$

and obtain

$$\int_0^1 dy 4R(\theta)y e^{-4\alpha R(\theta)y^2} \frac{\sin\{2(l+n)[\sin^{-1}(y)]\}}{l+n}.$$

$$(\text{A16})$$

Let $y = \sin\psi$ and $a = 4\alpha R(\theta)$:

$$\frac{1}{2\alpha} \int_0^{\pi/2} d\psi (a \sin 2\psi) e^{-a \sin^2\psi} \frac{\sin 2(l+n)\psi}{l+n}.$$

$$(\text{A17})$$

Integrating once by parts, we obtain

$$\frac{1}{\alpha} \int_0^{\pi/2} d\psi \cos 2(l+n)\psi e^{-a \sin^2\psi}.$$

$$(\text{A18})$$

Changing variables again ($2\psi = x$), we find

$$\frac{e^{-a/2}}{2\alpha} \int_0^{\pi} dx e^{(a/2)\cos x} \cos(l+n)x$$

$$= \frac{\pi}{2\alpha} e^{-a/2} e^{i\pi/2(l+n)} J_{l+n}(-ia/2).$$

Then, we have

$$\int_0^{\infty} dx e^{-2\alpha x} \frac{\sin(l+n)\varphi_m}{l+n}$$

$$= \frac{\pi}{2\alpha} e^{i(l+n)\pi/2} e^{-2\alpha R(\theta)} J_{l+n}(-i2\alpha R(\theta)). \quad (\text{A19})$$

Using similar manipulations, we can show that (A19) holds also for $l+n = 0$.

We have then for δY

$$\delta Y = \frac{3}{4\pi} \frac{Ne^2}{m\omega_c} \int_0^{\pi} d\theta \sin\theta \cos^2\theta e^{-2\alpha R(\theta)}$$

$$\times \frac{\pi}{\alpha} \sum_{n=-\infty}^{+\infty} \sum_{l=-\infty}^{+\infty} e^{i(n+l)\pi}$$

$$\times \frac{J_l(i\alpha R(\theta)) J_{l+n}(-i2\alpha R(\theta)) J_n(-i\alpha R(\theta))}{\gamma + in}. \quad (\text{A20})$$

Using the addition theorem⁸⁶ for Bessel functions

$$\sum_{l=-\infty}^{+\infty} e^{i(n+l)\pi} J_{l+n}(-i2\alpha R(\theta)) J_l(i\alpha R(\theta)) = J_n(i\alpha R(\theta)),$$

$$(\text{A21})$$

one finally obtains Eq. (15) in the text:

$$\delta Y^{zz} = \frac{Ne^2}{m\omega_c} \sum_{n=-\infty}^{+\infty} \frac{A_n^{zz}(\alpha, R_c)}{\gamma + in}, \quad (\text{A22})$$

where

$$A_n^{zz}(\alpha, R_c) = \frac{3}{4\alpha} \int_0^{\pi} d\theta \sin\theta \cos^2\theta e^{-2\alpha R(\theta)}$$

$$\times J_n(-i\alpha R(\theta)) J_n(i\alpha R(\theta)). \quad (\text{A23})$$

Similarly, we obtain for A_n^{yy} , used in the text, and for A_n^{xx} and A_n^{xy} , which are useful in a complete evaluation of the variational function,⁷³

$$A_n^{yy} = \frac{3}{4\alpha} \int_0^{\pi} d\theta \sin^3\theta e^{-2\alpha R(\theta)}$$

$$\times J_n'(-i\alpha R(\theta)) J_n'(i\alpha R(\theta)),$$

$$A_n^{xx} = \frac{3}{4\alpha} \int_0^{\pi} d\theta \sin^3\theta e^{-2\alpha R(\theta)} \frac{n^2}{\alpha^2 R(\theta)^2}$$

$$\times J_n(-i\alpha R(\theta)) J_n(i\alpha R(\theta)), \quad (\text{A24})$$

$$A_n^{xy} = \frac{3}{4\alpha} \int_0^{\pi} d\theta \sin^3\theta e^{-2\alpha R(\theta)} \frac{n}{\alpha R(\theta)}$$

$$\times J_n'(-i\alpha R(\theta)) J_n(i\alpha R(\theta)).$$

APPENDIX B: RESONANT NONLOCAL CONDUCTIVITY

Although not used in the text, we can generalize the results in Appendix A to obtain the resonant nonlocal conductivity for a semi-infinite metal with a diffuse surface. Using the concept of an image metal shown in Fig. (27), we can rewrite Maxwell's equations for a diffuse surface as³⁸

$$-k^2 E^z(k) = \frac{E^z(0)'}{\pi} + i\omega\mu_0 \int_{-\infty}^{+\infty} dq'$$

$$\times [\sigma_r(k, k') + \sigma_n(k, k')] E^z(k'), \quad (\text{B1})$$

where $E^z(0)'$ is the derivative of electric field at the surface. $\sigma_r(k, k')$ and $\sigma_n(k, k')$ are the resonant

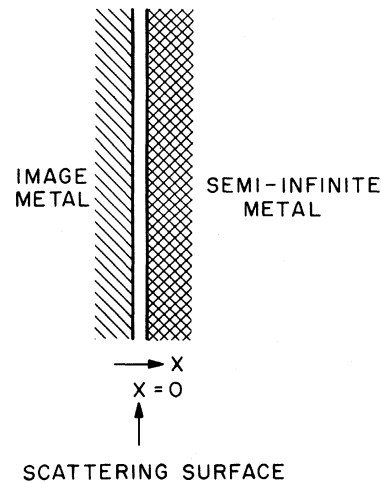


FIG. 27. Image metal concept (Ref. 38).

and nonresonant nonlocal conductivities. The exact solution to (B1) is the solution of the surface impedance problem for $\vec{E} \parallel \vec{H}$ with a diffuse surface scattering and would enable a detailed fit between theory and experiment. The solution of course does not exist at present. In the following we derive an expression for part of the integrand in (B1), namely, $\sigma_r(k, k')$.

$\sigma_r(k, k')$ is defined to give the k th Fourier component of the current $J(k)$ given a distribution func-

tion of electric fields $E(k')$:

$$J^x(k) = \int_{-\infty}^{+\infty} dk' \sigma_r^{xx}(k, k') E^x(k'). \quad (\text{B2})$$

We define $\sigma_r(k, k')$ as that part of the conductivity caused by the electrons that do not hit the surface.

The solution is found by assuming an exponential field $E(x) = e^{-ikx - |x|s}$, performing the same manipulations for the semi-infinite metal and its image as were done in Appendix A, and then letting $s \rightarrow 0$. One obtains in a straightforward manner

$$\begin{aligned} \sigma_r^{xx}(k, k') = & \frac{3}{2} \frac{Ne^2}{m\omega_c} \int_0^\pi d\theta \sin\theta \cos^2\theta \sum_n \frac{J_n(kR(\theta))J_n(k'R(\theta))}{\gamma + in} \delta(k - k') \\ & - \frac{3}{2} \frac{Ne^2}{m\omega_c} \int_0^\pi d\theta \sin\theta \cos^2\theta \sum_n \frac{J_n(kR(\theta))J_n(k'R(\theta))}{\gamma + in} \frac{\sin(k' - k)R(\theta)}{\pi(k' - k)}. \quad (\text{B3}) \end{aligned}$$

The first term is just the bulk nonlocal conductivity, whereas the second is the surface term. The surface term operates to remove from resonance those bulk electrons that no longer can resonate

because of the presence of the surface. It is of course not diagonal in k . Similar expressions for the other components of the conductivity tensor can be obtained, but we do not write them here.

¹L. D. Landau, Zh. Eksp. Teor. Fiz. **30**, 1058 (1956) [Sov. Phys.-JETP **3**, 920 (1957)].

²V. P. Silin, Zh. Eksp. Teor. Fiz. **33**, 495 (1957) [Sov. Phys.-JETP **6**, 387 (1958)].

³W. M. Walsh, Jr. and P. M. Platzman, Phys. Rev. Lett. **15**, 784 (1965).

⁴P. M. Platzman and W. M. Walsh, Jr., Phys. Rev. Lett. **19**, 514 (1967); Phys. Rev. Lett. **20**, 89E (1968).

⁵P. M. Platzman, W. M. Walsh, Jr., and E. Ni Foo, Phys. Rev. **172**, 689 (1968).

⁶S. Schultz and G. Dumifer, Phys. Rev. Lett. **18**, 283 (1967).

⁷J. R. Schrieffer, *Theory of Superconductivity* (Benjamin, New York, 1964).

⁸R. E. Prange and A. Sachs, Phys. Rev. **158**, 672 (1967).

⁹V. Heine, P. Nozieres, and J. W. Wilkins, Philos. Mag. **13**, 741 (1966).

¹⁰M. Ya. Azbel' and E. A. Kaner, Zh. Eksp. Teor. Fiz. **30**, 811 (1956) [Sov. Phys.-JETP **3**, 772 (1956)].

¹¹H. Scher and T. Holstein, Phys. Rev. **148**, 598 (1966).

¹²P. B. Allen, in *Proceedings of the Twelfth International Conference on Low-Temperature Physics* (Academic Press of Japan, Tokyo, 1970), p. 517.

¹³W. L. McMillan and J. M. Rowell, in *Superconductivity*, edited by R. D. Parks (Marcel Dekker, New York, 1969), Chap. 11.

¹⁴G. Grimvall, Phys. Kondens. Mater. **9**, 283 (1969); J. Phys. Chem. Solids **29**, 1221 (1968).

¹⁵J. F. Koch and R. E. Doezema, Phys. Rev. Lett. **24**, 507 (1970).

¹⁶P. Haussler and S. J. Welles, Phys. Rev. **152**, 675 (1966).

¹⁷T. W. Moore, Phys. Rev. Lett. **16**, 581 (1966).

¹⁸J. J. Sabo, Phys. Rev. B **1**, 1325 (1970); P. B. Allen and M. L. Cohen, Phys. Rev. B **1**, 1329 (1970).

¹⁹P. Goy, Phys. Lett. A **31**, 584 (1970); Phys. Lett. A **32**, 474 (1970); P. Goy and G. Weisbuch, Phys. Rev. Lett. **25**, 225 (1970).

²⁰R. G. Poulsen and W. R. Datars, Solid State Commun. **8**, 1969 (1970).

²¹I. Krasnopolin and M. S. Khaikin, Zh. Eksp. Teor. Fiz. Pis'ma Red. **12**, 76 (1970) [JETP Lett. **12**, 54 (1970)].

²²R. R. Joyce and P. L. Richards, Phys. Rev. Lett. **24**, 1007 (1970); G. Brandli, Phys. Rev. Lett. **28**, 159 (1972).

²³T. Holstein, Phys. Rev. **96**, 535 (1954).

²⁴P. Goy and B. Gastaing, in *Proceedings of the Thirteenth International Conference on Low Temperature Physics*, Boulder, 1972 (unpublished).

²⁵R. C. Dynes and J. P. Carbotte, Phys. Rev. **175**, 913 (1968).

²⁶J. P. Carbotte, R. C. Dynes, and P. N. Trofimenkoff, Can. J. Phys. **47**, 1107 (1969).

²⁷J. S. Dugdale and D. Gugan, Proc. R. Soc. A **270**, 186 (1962).

²⁸J. W. Ekin, Phys. Rev. Lett. **26**, 1550 (1971).

²⁹J. W. Ekin and B. W. Maxfield, Phys. Rev. B **4**, 4215 (1971).

³⁰B. Hayman and J. P. Carbotte, Can. J. Phys. **49**, 1952 (1971).

³¹T. M. Rice and L. J. Sham, Phys. Rev. B **1**, 4546 (1970).

³²C. R. Leavens and J. P. Carbotte (unpublished).

³³T. M. Rice, Phys. Rev. **175**, 858 (1968), and references therein.

³⁴P. B. Allen and M. J. G. Lee, Phys. Rev. B **5**, 3848 (1972), and references therein.

³⁵C. C. Grimes and A. F. Kip, Phys. Rev. **132**, 1991 (1963).

³⁶D. Shoenberg and P. J. Stiles, Proc. R. Soc. A **281**, 62 (1964).

³⁷W. M. Walsh, Jr. (private communication).

³⁸R. G. Chambers, in *The Physics of Metals*, edited by J. M. Ziman (Cambridge U. P., Cambridge, England, 1969), Chap. 4.

³⁹H. D. Drew, Phys. Rev. B **5**, 360 (1972).

⁴⁰B. E. Meierovich, Zh. Eksp. Teor. Fiz. **58**, 1412 (1970) [Sov. Phys.-JETP **31**, 756 (1970)].

⁴¹A. Kamgar, J. O. Henningsen, and J. F. Koch, Phys. Rev. B **6**, 342 (1972).

⁴²S. J. Allen, Jr., Bull. Am. Phys. Soc. **17**, 41 (1972).

⁴³S. J. Allen, Jr., Bull. Am. Phys. Soc. **16**, 104 (1971).

- ⁴⁴R. E. Glover, III and M. Tinkham, Phys. Rev. **104**, 844 (1956).
- ⁴⁵R. E. Glover, III and M. Tinkham, Phys. Rev. **108**, 243 (1957).
- ⁴⁶P. L. Richards and M. Tinkham, Phys. Rev. **119**, 575 (1960).
- ⁴⁷S. L. Norman and D. H. Doubllass, Jr., Phys. Rev. Lett. **17**, 875 (1966); Phys. Rev. Lett. **18**, 339 (1967).
- ⁴⁸P. Goy and G. Weisbuch, Phys. Kondens. Mater. **9**, 200 (1969).
- ⁴⁹H. D. Drew and A. J. Sievers, Phys. Rev. Lett. **19**, 697 (1967); A. J. Sievers, J. Appl. Phys. **41**, 980 (1970).
- ⁵⁰U. Strom, H. D. Drew, and J. F. Koch, Phys. Rev. Lett. **26**, 1110 (1971).
- ⁵¹H. A. Gebbie, N. W. B. Stone, and F. D. Findlay, Nature (Lond.) **202**, 685 (1964).
- ⁵²L. E. S. Mathias, H. Crocker, and M. S. Wills, Electron. Lett. **1**, 45 (1965).
- ⁵³D. R. Lide, Jr. and A. G. Maki, Appl. Phys. Lett. **11**, 62 (1967).
- ⁵⁴A. G. Maki, Appl. Phys. Lett. **12**, 122 (1968).
- ⁵⁵W. S. Benedict, M. A. Pollack, and W. J. Tomlinson, III, IEEE J. Quantum Electron. **5**, 108 (1969), and references therein. We would like to thank M. A. Pollack for advising us on the construction and operation of the laser.
- ⁵⁶Buckbee-Mears Co., ruling No. 1004.
- ⁵⁷G. D. Boyd and J. P. Gordon, Bell Syst. Tech. J. **40**, 489 (1961).
- ⁵⁸R. Ulrich, K. F. Renk, and L. Genzel, IEEE Trans. Microwave Theory Tech. **11**, 363 (1963).
- ⁵⁹N. Marcuvitz, *Waveguide Handbook*, MIT Rad. Lab. Series (McGraw-Hill, New York, 1951), Vol. 10, p. 280.
- ⁶⁰The grid is used at 4.2 °K in the far infrared where the classical expression for Cu conductivity fails. Using the classical treatment and an infinite conductivity, one attains a reflectivity from the screen of ≈ 0.999 (see Ref. 19).
- ⁶¹F. J. Low, J. Opt. Soc. Am. **51**, 1300 (1961).
- ⁶²F. DeRosa (unpublished).
- ⁶³R. C. Chlman, P. L. Richards, and M. Tinkham, J. Opt. Soc. Am. **48**, 531 (1958).
- ⁶⁴G. Goubau and F. Schwing, IRE Trans. Antennas Propag. **9**, 248 (1961); J. R. Christian and G. Goubau, IRE Trans. Antennas Propag. **9**, 256 (1961); J. B. Beyer and E. H. Scheibe, IEEE Trans. Microwave Theory Tech. **11**, 18 (1963).
- ⁶⁵J. F. Koch, R. A. Stradling, and A. F. Kip, Phys. Rev. **133**, A240 (1964).
- ⁶⁶P. B. Miller and R. R. Haering, Phys. Rev. **128**, 126 (1962).
- ⁶⁷For a recent review see Ref. 39.
- ⁶⁸M. Ya. Azbel' and E. A. Kaner, Zh. Eksp. Teor. Fiz. **32**, 896 (1957) [Sov. Phys.-JETP **5**, 730 (1957)]; J. Phys. Chem. Solids **6**, 113 (1958).
- ⁶⁹R. G. Chambers, Proc. Phys. Soc. Lond. **86**, 305 (1965).
- ⁷⁰L. E. Hartman and J. M. Luttinger, Phys. Rev. **151**, 430 (1966); Phys. Rev. **156**, 1038 (1961).
- ⁷¹P. M. Marcus, Circ. U.S. Natl. Bur. Stand. **519**, 265 (1952).
- ⁷²R. E. Prange and T-W Nee, Phys. Rev. **168**, 779 (1968).
- ⁷³M. C. Jones and E. H. Sondheimer, Proc. R. Soc. A **278**, 256 (1964).
- ⁷⁴G. A. Baraff, Phys. Rev. **187**, 851 (1969).
- ⁷⁵V. Heine and I. Abarenkov, Philos. Mag. **9**, 451 (1964).
- ⁷⁶A. D. E. Animalu and V. Heine, Philos. Mag. **12**, 1249 (1965).
- ⁷⁷W. A. Harrison, *Pseudopotentials in the Theory of Metals* (Benjamin, New York, 1966).
- ⁷⁸R. A. Cowley, A. D. B. Woods, and G. Dollin, Phys. Rev. **150**, 487 (1966).
- ⁷⁹W. M. Walsh, Jr., P. M. Platzman, P. S. Peercy, L. W. Rupp, Jr., and P. H. Schmidt, in Ref. 12, p. 619.
- ⁸⁰G. L. Dunifer, P. H. Schmidt, and W. M. Walsh, Jr., Phys. Rev. Lett. **26**, 1553 (1971).
- ⁸¹E-Ni Foo, Phys. Rev. **182**, 674 (1969).
- ⁸²G. L. Dunifer kindly provided the computer program for E.I.H.
- ⁸³N. V. Brotzyna and V. G. Skobov, Zh. Eksp. Teor. Fiz. **56**, 694 (1969) [Sov. Phys.-JETP **29**, 379 (1969)].
- ⁸⁴E. A. Kaner and V. G. Skobov, Fiz. Tverd. Tela **6**, 1104 (1964) [Sov. Phys.-Solid State **6**, 851 (1964)].
- ⁸⁵N. W. Ashcroft, Phys. Lett. **23**, 48 (1966).
- ⁸⁶G. H. Watson, *Theory of Bessel Functions* (Cambridge U. P., Cambridge, England, 1944).